NASA CR 54764
AGC 8800-12

AERODYNAMIC DESIGN AND ESTIMATED PERFORMANCE OF A TWO-STAGE CURTIS TURBINE FOR THE LIQUID OXYGEN TURBOPUMP OF THE M-1 ENGINE

By

R. Beer

Prepared for

National Aeronautics and Space Administration

Contract NAS 3-2555

AEROJET-GENERAL CORPORATION

SACRAMENTO, CALIFORNIA

NASA CR-54764
AGC 8800-12

TECHNOLOGY REPORT

AERODYNAMIC DESIGN AND ESTIMATED PERFORMANCE OF A TWO-STAGE CURTIS TURBINE FOR THE LIQUID OXYGEN TURBOPUMP OF THE M-1 ENGINE

Prepared For

NATIONAL AERONAUTICS AND SPACE ADMINISTRATION

19 November 1965

CONTRACT NAS3-2555

PREPARED BY:
AEROJET-GENERAL CORPORATION
LIQUID ROCKET OPERATIONS
SACRAMENTO, CALIFORNIA

AUTHOR: R. Beer

APPROVED: W. E. Campbell
Assistant Manager
M-1 Turbopump Project

TECHNICAL MANAGEMENT:
NASA LEWIS RESEARCH CENTER
CLEVELAND, OHIO

TECHNICAL MANAGER: W. W. Wilcox

APPROVED: W. F. Dankhoff
M-1 Project Manager

ABSTRACT

14235

A two-stage Curtis turbine was designed for use in the oxidizer turbopump of the M-1 Engine.

At its design point, the turbine produces 26,800 horsepower at a velocity ratio of .133 and an estimated efficiency of .53.

Blunt edged turbine rotor airfoils are used throughout. Beside superior performance at subsonic Mach numbers, these airfoils (in the form of hollow sheet metal blades) offer advantages in fabricability, thermal fatigue resistance, and weight savings as compared to airfoils with sharp leading and trailing edges.

TABLE OF CONTENTS

LIST OF TABLES

LIST OF FIGURES

LIST OF FIGURES (CONT'D)

I. SUMMARY

This report delineates the aero-thermodynamic design of a Curtis turbine designed for the oxidizer turbopump of the M-1 Engine. At the design point, the turbine produces 26,800 horsepower at an estimated efficiency of 53%.

The turbine design parameters are:

Inlet total pressure (at nozzle inlet)	psia	200
Inlet total temperature (at nozzle inlet)	°R	1190
Outlet static pressure	psia	120
Pressure ratio, total to static	---	1.67
Mass flow	lb/sec	115
Speed	rpm	3635
Mean diameter of first stage	in.	33.00
Blade-jet speed ratio	---	.133

Blunt edged turbine rotor airfoils are used throughout. Besides superior performance at subsonic Mach numbers, these airfoils (in the form of hollow sheet metal blades) offer advantages in fabricability, thermal fatigue resistance, and weight savings as compared to airfoils with sharp leading and trailing edges.

II. INTRODUCTION

The pumping system of the liquid propellant M-1 engine consists of two separate turbopumps, each having a direct-drive turbine. A gas generator, separate from the main engine, supplies the turbines, which are arranged in series, with the combustion products of liquid hydrogen and liquid oxygen. The gas is initially expanded in the fuel turbine and then further expanded in the oxidizer turbine. The exhaust from the oxidizer turbine is used in three heat exchangers; to heat hydrogen for the gimbal actuators, and to heat hydrogen and oxygen for tank pressurization. The oxidizer exhaust is then used to cool the lower section of the skirt of the main nozzle. Finally, the exhaust is ejected via a set of small nozzles to provide an approximate specific impulse of 260 $\frac{\text{lbf-sec}}{\text{lbm}}$ (See Figure 1).

Initially, single stage turbines were designed for the fuel and oxidizer turbopumps. The single stage turbine rotor for the liquid oxygen turbopump was fabricated from a solid forging and was used in the initial test series as a workhorse model. For the development engine a two-stage Curtis Turbine was specified and the aerodynamic design of this unit is the subject of this report. This turbine has not been tested full scale under hot conditions. However, actual experimental performance data of the inlet manifold, turbine nozzle, and complete two-stage turbine has been obtained in cold air on a subscale model at Lewis Research Center. This effort will be reported separately by NASA. In addition, the fabrication methods used on both rotors and stators, and the design and fabrication of the unique integrated pump backplate-turbine inlet manifold will be discussed in separate contractor reports.

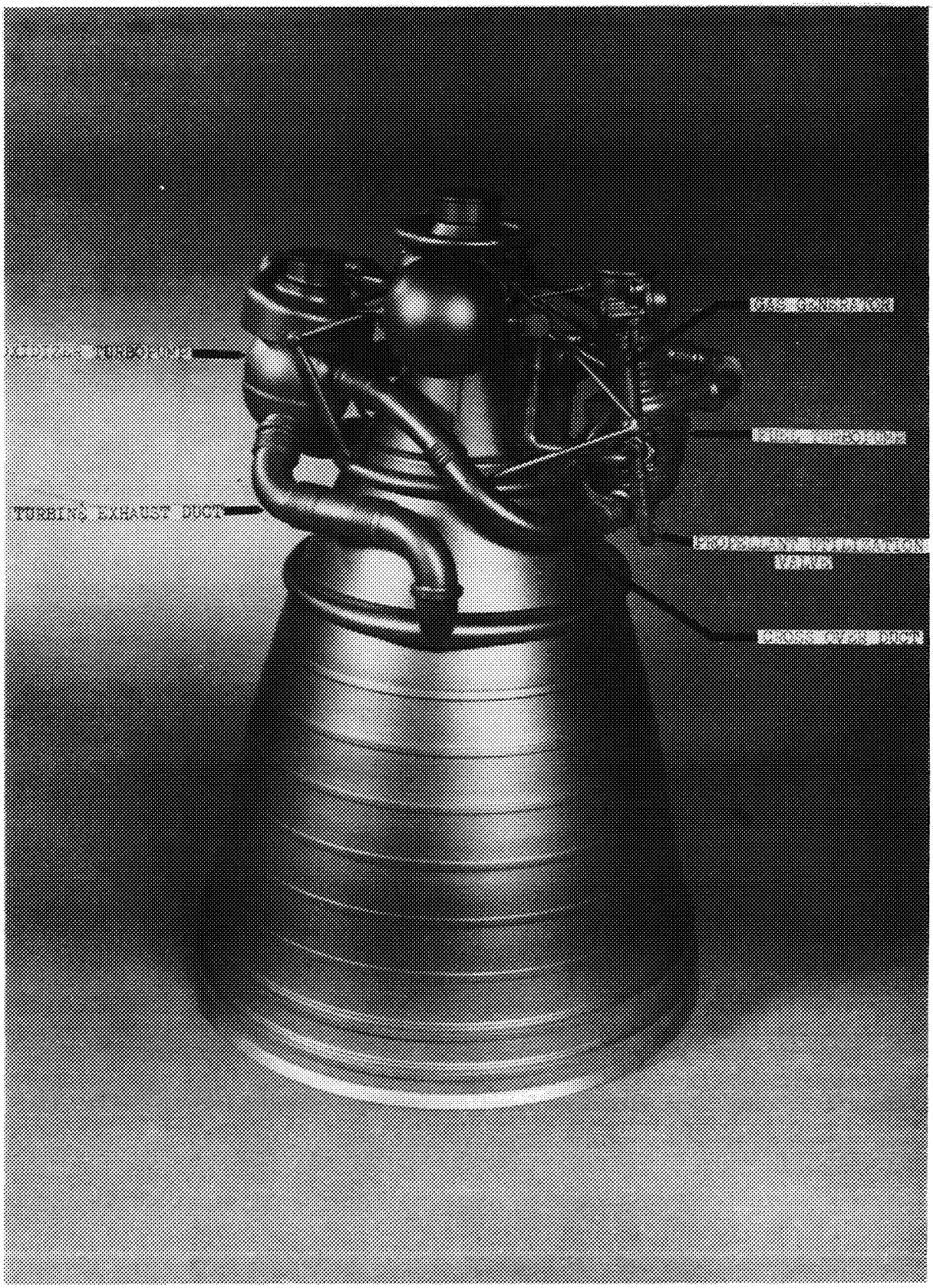

Figure 1. M-1 Engine Mockup

The nozzle, reversing vane and rotor assemblies were fabricated entirely from Inconel 718 component parts and weld assembled by the process of Electron Beam Welding. Figures 2, 3 and 4 show photographs of the nozzle assembly (Figure 2), the reversing vane assembly (Figure 3) and the dual rotor assembly mounted to hub and shaft. (Figure 4)

III. DESIGN

A. REQUIREMENTS AND GAS PROPERTIES

Figure 1 shows a photograph of the engine mockup indicating the ducting elements. At the design point, 14% of the total flow available from the gas generator (to drive both turbines) by-passes the fuel turbine. The by-pass flow and the fuel turbine exhaust flow are carried through two 11.4-in. (inside diameter) cross-over ducts to the oxidizer turbine inlet manifold. This manifold is considered to be part of the ducting and the turbine inlet conditions specified in this report apply to the annulus directly upstream from the nozzles. It is assumed that the manifold provides uniform nozzle inlet conditions over the entire circumference.

An engine system balance was performed based upon an assumed variation of the turbine efficiency versus the velocity ratio (U/Co) as shown on Figure 5 and upon estimated cross-over duct pressure losses. This engine system balance resulted in the design parameters presented as Table 1.

The properties of the turbine gas, which is the combustion product of liquid hydrogen and liquid oxygen, are shown as Figure 6. The effect of the pressure upon c_p and γ is neglected. Also, c_p and γ are taken at the reference temperature of 1130°R and kept constant throughout the turbine. The gas properties used are as follows:

O/F	.8	---
c_p	1.984	BTU/lbm-°R
γ	1.382	---
$\frac{\gamma-1}{\gamma}$	.2765	---
$\frac{\gamma}{\gamma-1}$	3.62	---
R	426	$\frac{\text{lbf-ft}}{\text{lbm-°R}}$

B. DESIGN PHILOSOPHY

The maximum total-to-static efficiency of a turbine stage is predominantly a function of the U/Co ratio of the stage. At different U/Co ratios, maximum efficiencies are obtained with different reaction distributions between stator and rotor. Figure 7 (1) shows the efficiency of a two stage Curtis turbine versus Co/U and reaction distribution. For $U/C_o = 0.133$ or $Co/U = 7.5$, the

(1) Flugel, Gustav, Die Dampfturbinen, ihre Berechnung und Konstruktion mit einem Anhang uber die Gasturbinen, Johann Ambrosius Barth, Leipzig, 1931, page 87

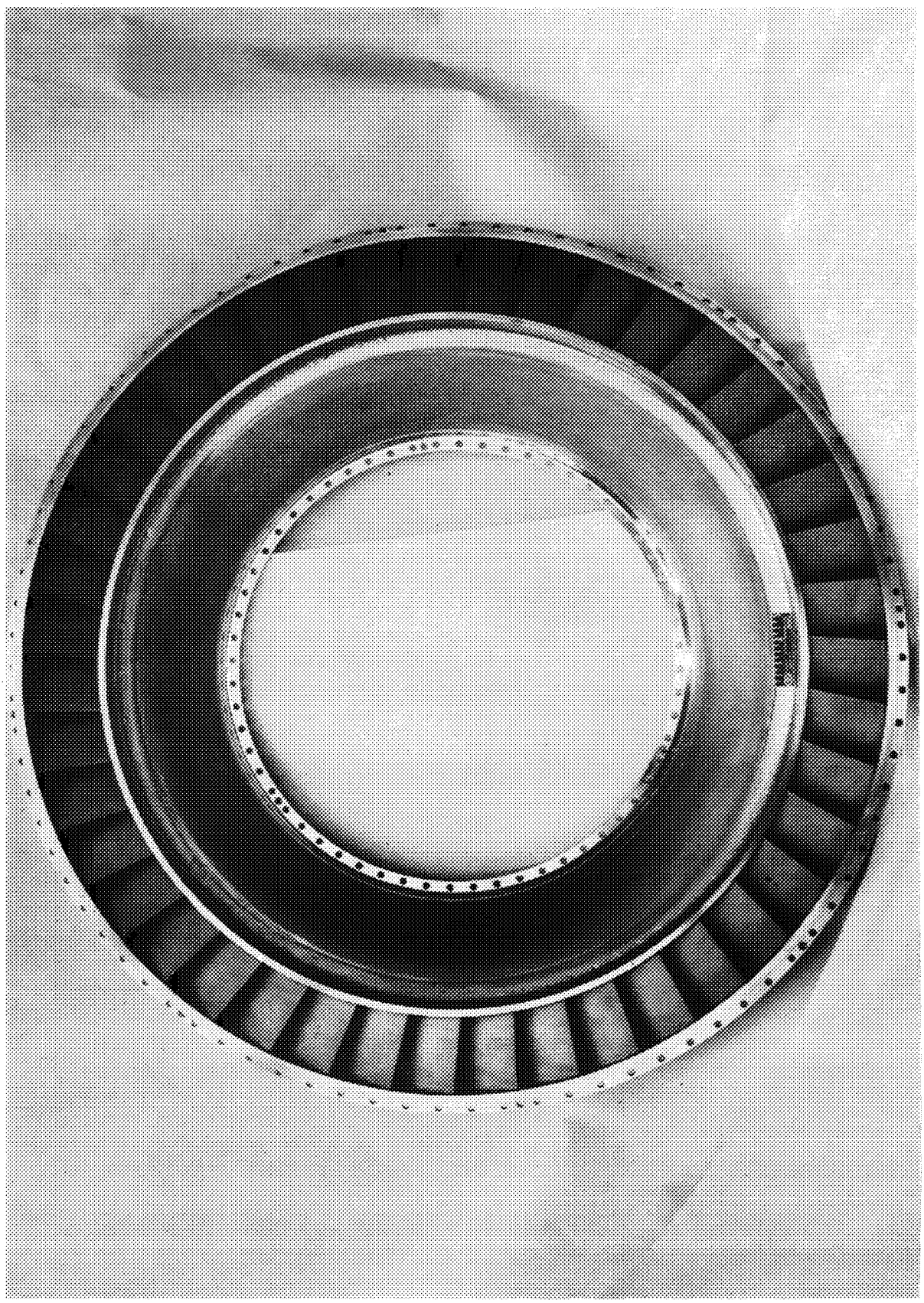

Figure 2. Nozzle Assembly

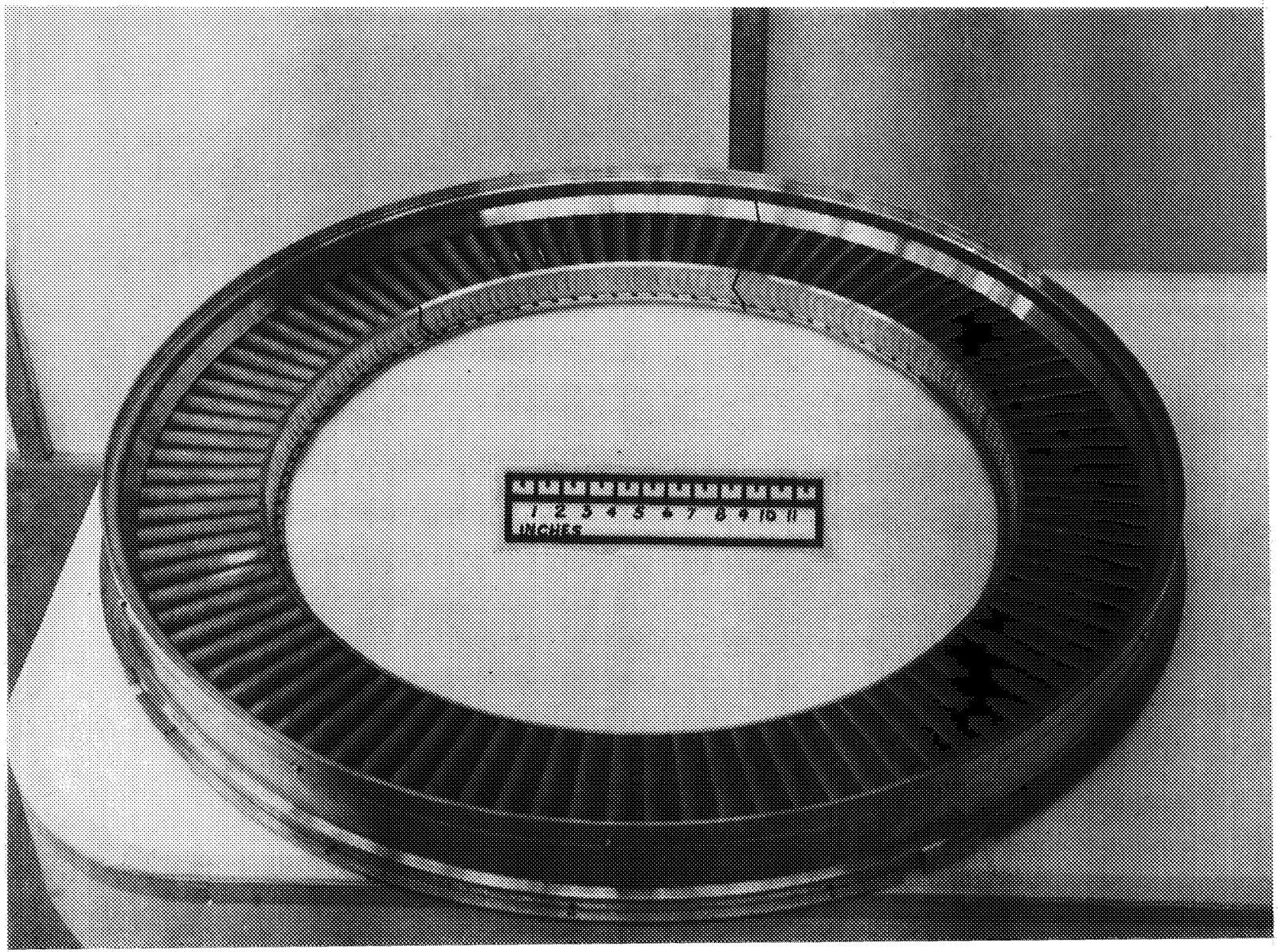

Figure 3. Reversing Vane Assembly

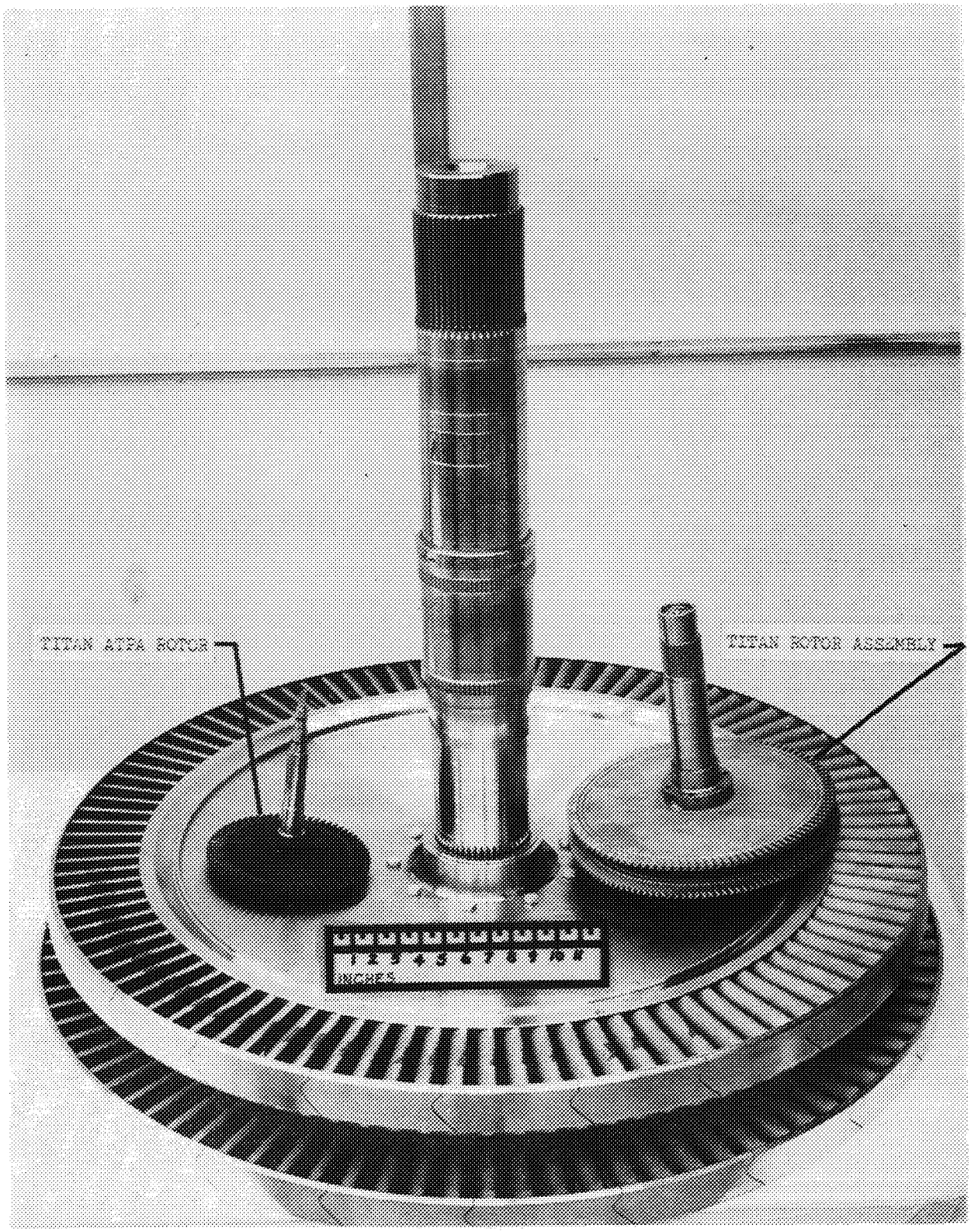

Figure 4. Rotor Assembly

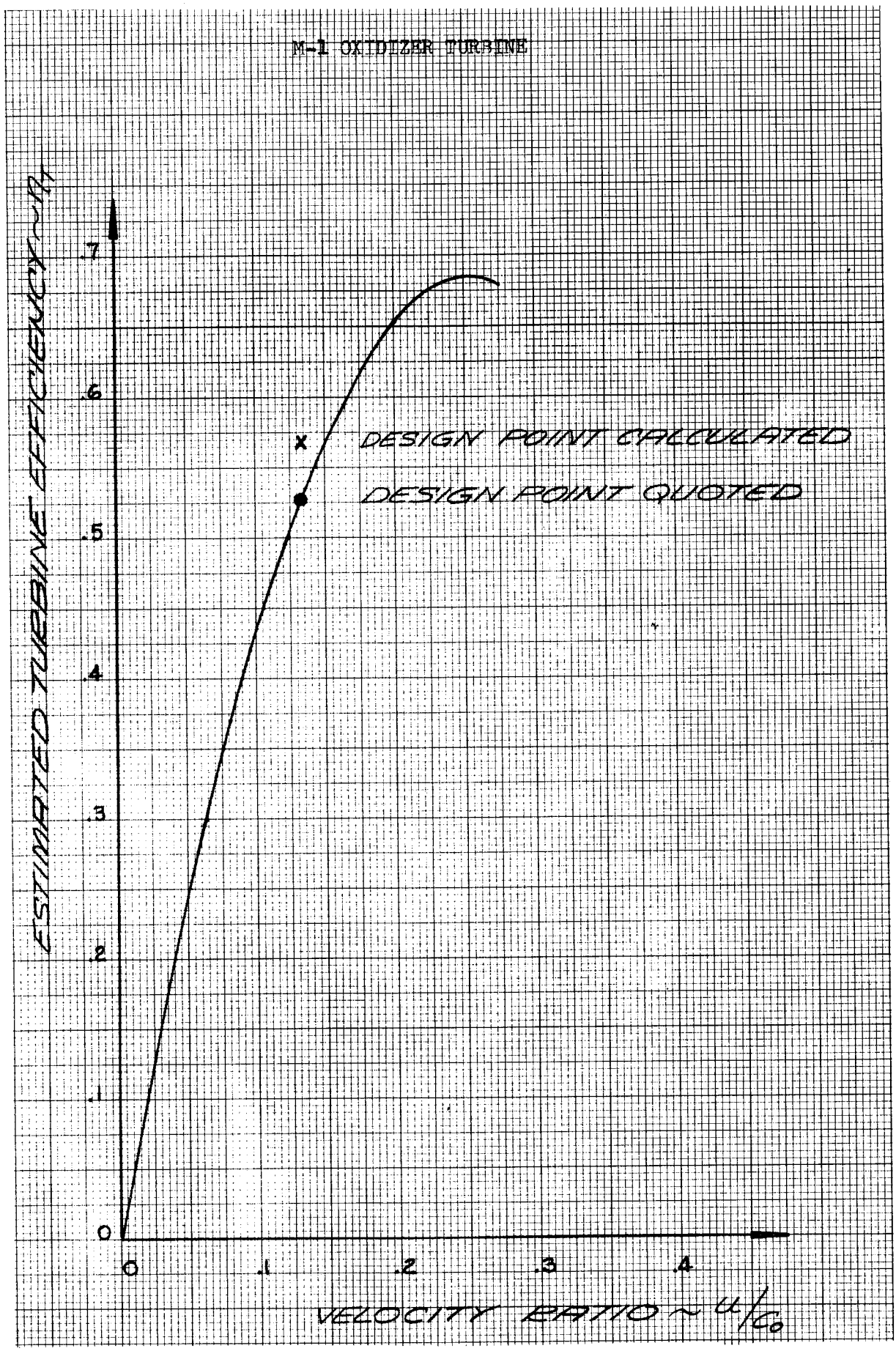

Figure 5. Estimated Turbine Efficiency vs Velocity Ratio

TABLE 1

M-1 ENGINE

LIQUID OXYGEN TURBOPUMP

TURBINE DESIGN PARAMETERS

Inlet Total Pressure (at nozzle inlet)	psia	200
Inlet Total Temperature (at nozzle inlet)	R	1190
Outlet Static Pressure	psia	120
Pressure Ratio, Total-to-Static	---	1.67
Mass Flow	lb/sec	115
Speed	rpm	3635
Mean Diameter of First Stage	in.	33.00
Blade-Jet Speed Ratio	---	.133

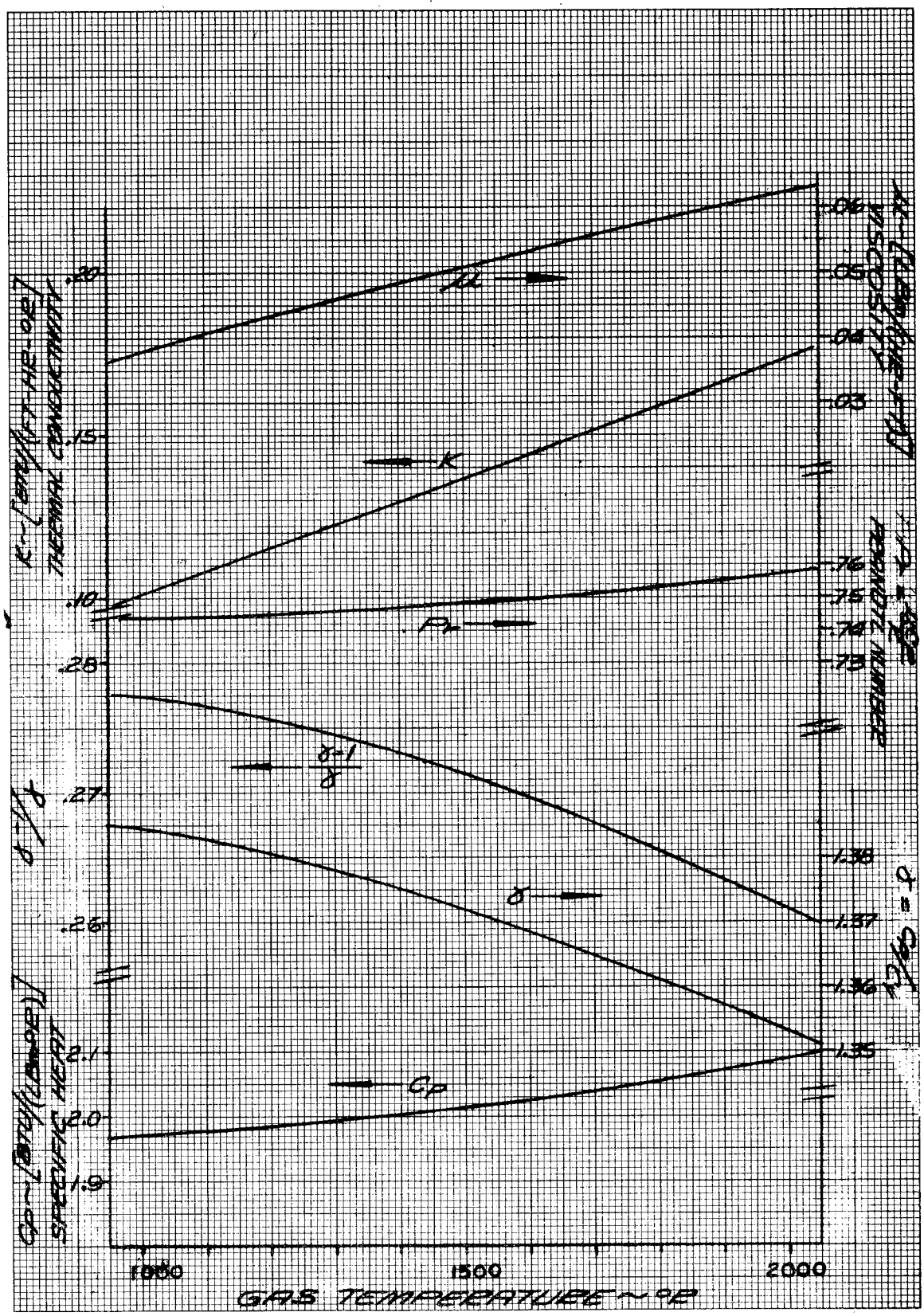

Figure 6. Properties of Combustion Products of Hydrogen and Oxygen for a Mixture Ratio O/F = .8 and M = 3.63,

$$R = 426 \frac{\text{lbf - ft}}{\text{lbm - °R}}$$

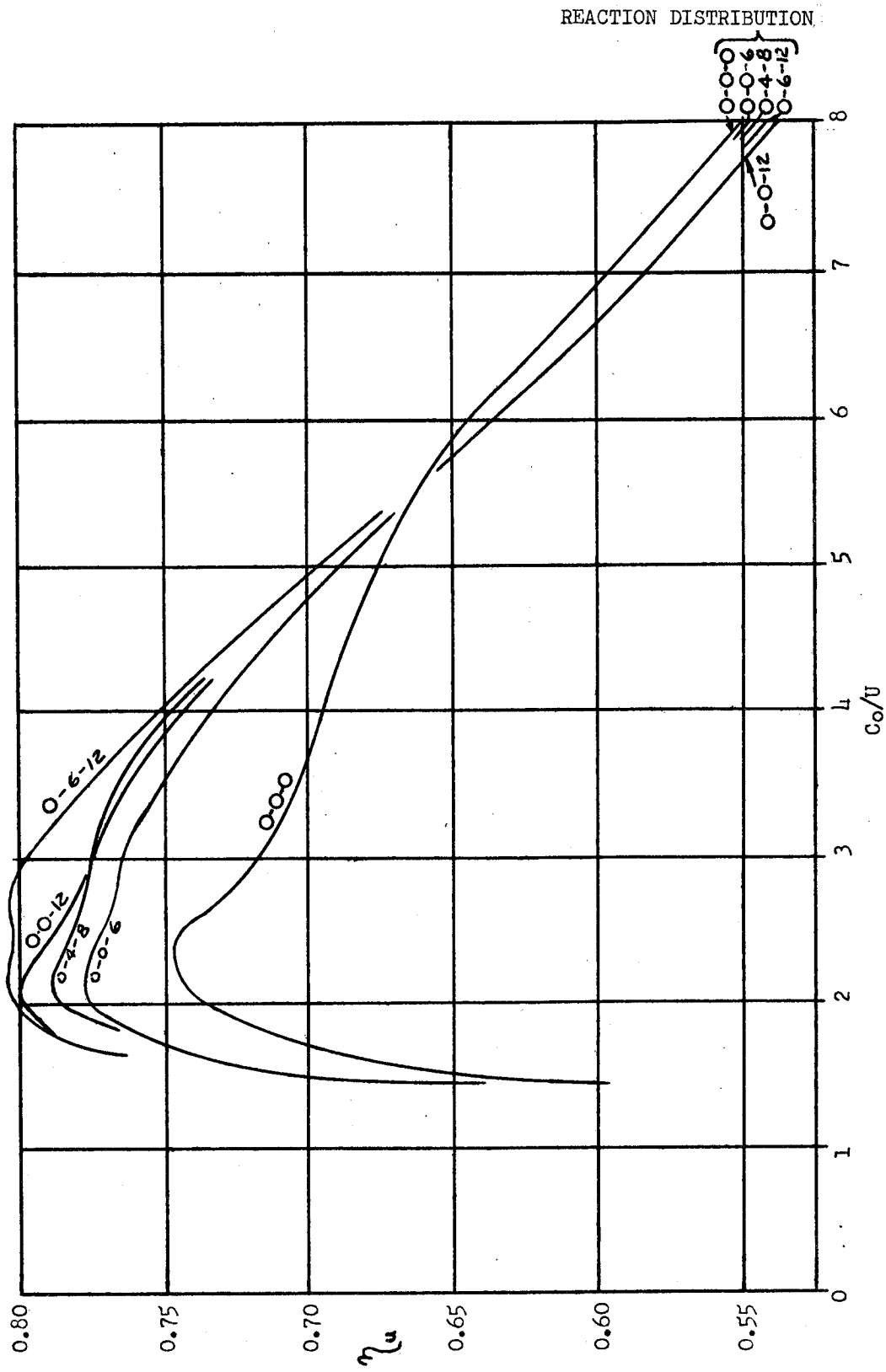

Figure 7. Efficiency of Two-Stage Curtis Turbines vs Co/U and Reaction Distribution

reaction distribution 0-0-0 is recommended. This means that the entire static pressure drop (or static enthalpy drop) is taken in the nozzle of the first stage and no static enthalpy drops occur in the rotors of the first and second stages and reversing vanes. However, preliminary calculations indicated that this reaction distribution results in undesirably long blades in the second rotor.

The reaction distribution finally selected, 0-3-7, has no enthalpy drop in the first stage rotor, 3% of over-all available enthalpy drop in the reversing vanes and 7% of over-all available enthalpy drop in the second stage rotor. This results in desired blade heights with only a small loss in performance.

C. AERO-THERMODYNAMIC DESIGN

1. Flow Quantities at Mean Diameter

a. Loss Estimate

It appeared that the rotor velocity coefficients, previously used at Aerojet-General in the design of turbines, were too conservative for the M-1 Engine oxidizer turbine. This M-1 oxidizer turbine has a nozzle height in excess of 3-in., a rotor blade width of approximately 1.5-in., and only subsonic velocities throughout its blading. It is expected to have high blading efficiencies. Because information concerning the losses in turbine bladings similar to the ones to be designed were not available, a published method of loss estimation was selected(2). This method for loss estimation is summarized in Appendix B.

Prior to the selection of this method, the velocity coefficient of the rotor blade shown in Figure 8 was calculated using five different methods for comparison purposes. The results were as follows:

	$K_R = W_4/W_4'$
Stenning(3)	.94
Traupel(4)	.90
Vavra(5)	.86
Aerojet-General (Figure 9)	.835
Ainley(6) (extrapolated)	.80

Traupel provides the most realistic answer and his method was selected as mentioned above.

(2) Traupel, Walter, Thermische Turbomaschinen, Erster Band, Springer Verlag/ Berlin/Gottingen/Heidelberg, 1958
(3) Stenning, Alan H., Design of Turbines for High-Energy-Fuel-Low-Power-Output Applications, MIT Report No. 79
(4) Traupel, Walter, op. cit.
(5) Vavra, M. H., Analysis and Design of Modified 87-5 Turbine, AGLR No. 3, April 1962
(6) Ainley, D. G. and Mathieson, G. C. R., A Method of Performance Estimation for Axial-Flow Turbines, R&M 2974, December 1951

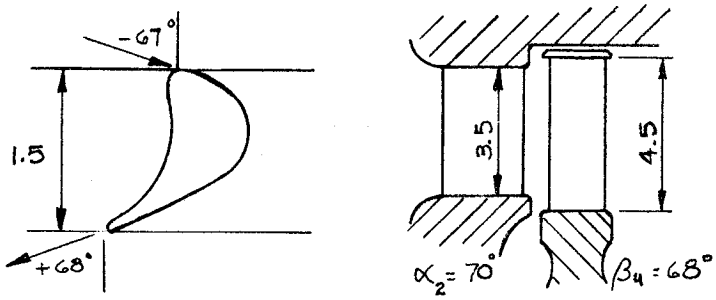

$Re_c = 8.3.10^5$

$Re_{Dh} = 3.0.10^5$

$M^* = .67$

Figure 8. Blade Configuration Used to Compare Different Methods for the Loss Prediction of a Rotor Blading

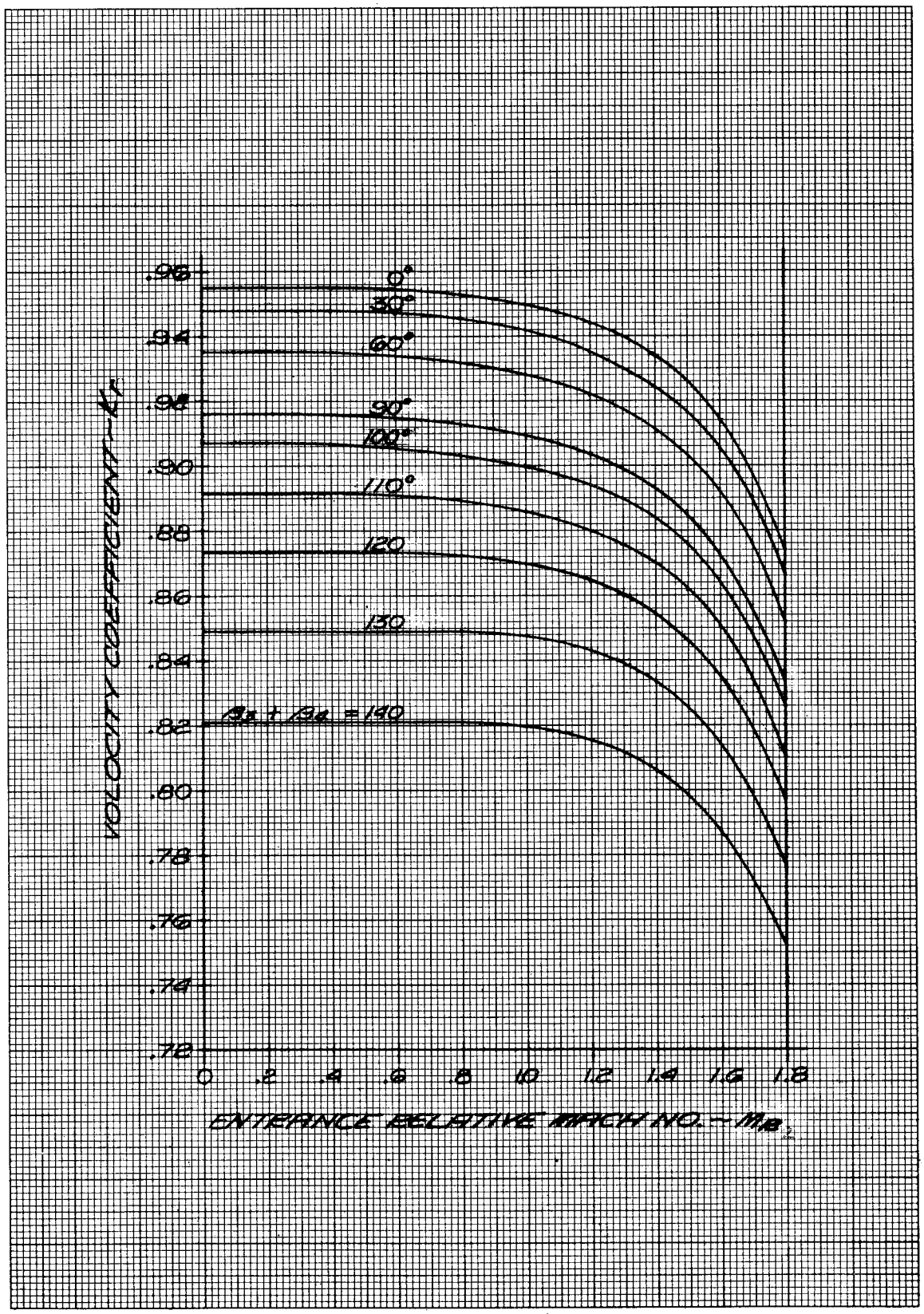

Figure 9. Rotor Velocity Loss Coefficient for Impulse Turbines

b. Performance

Based upon the loss estimation discussed in the preceding section, the expansion process in the T-S Chart and the velocity triangles were calculated for the mean diameter. The pertinent results from these calculations are provided as Table 2. Figure 10 shows the process in the T-S Chart and Figure 11 shows the velocity triangles at the mean diameter. A total-to-static efficiency of 56.7% was obtained from these calculations. This appears to represent the potential for this design after some development. Therefore, it was decided to use 53.0% as a conservative estimate for the engine system balance (see Figure 5). These efficiencies are based upon the seal arrangement shown in Figure 12 with axial clearances, k_a, of not larger than .100-in.

2. Flow Quantities at Hub and Tip

An untwisted sheet metal blade of constant cross-section was selected for all blade rows. As a result, the gas outlet angle of each blade row is nearly constant from hub to tip. The flow quantities at hub and tip were calculated from radial equilibrium considerations, assuming constant gas outlet angles, and using the method given by Traupel(7). The flow efficiencies were assumed to be constant from hub to tip. Results are presented in Table 3 and Figure 13. The loss coefficients used in the radial equilibrium calculations differ from those used in the performance calculations because the flow quantities at the hub and tip were calculated for a preliminary configuration which differed slightly from the final design selected. However, in view of the slight difference it was not considered necessary to recalculate the flow quantities at the hub and tip for the final configuration.

D. BLADE DESIGN

1. Solidity

The loss system detailed in Appendix B requires that optimum solidities be used as shown on Figure B-2 of that appendix. Actual and optimum solidities for the four blade rows are as follows:

	Nozzle	First Rotor	Rev. Row	Second Rotor
Number of Blades	43	98	97	94
Actual	1.54	1.525	1.51	1.46
Optimum	1.22-1.42	1.47-1.80	1.46-1.78	1.44-1.76

(7) Traupel, Walter, op. cit.

TABLE 2

FLOW QUANTITIES AT THE MEAN DIAMETER

	Dim	Nozzle Inlet	Nozzle Outlet	Rotor I Outlet	Rev.Vane Outlet	Rotor II Outlet
P_T	psia	200	193.0	151.2	146.1	128.2
P_{TR}	psia	-	174.5	163.2	137.5	134.6
T_T	°R	1190	1190	1133.3	1133.3	1099.5
T_{TR}	°R	-	1157.5	1157.5	1114.7	1114.7
T_s	°R	-	1061	1080.3	1085.5	1080.3
P_s	psia	-	126.8	126.8	124.8	120.0
V	ft/sec	$\simeq$ 0	3575	2290	2172	1388
U	ft/sec		524	524	524	520
W	ft/sec		3090	2765	1700	1850
α	degrees	$\simeq$ 90	70.00	-63.10	67.00	-56.50
β	degrees	-	66.65	-68.00	60.10	-65.50
D_m	inch	33	33.00	33.00	33.00	32.80
h_d	inch	-	3.20	3.90	4.80	5.55
Δ_b	inch	-	.400	.500	.400	-
M	-	-	.800	.509	.481	.309
M_R	-	-	.693	.614	.377	.410
ρ	lbm/ft^3	-	.0407	.0401	.0392	.0379

		STAGE I	STAGE II
L_u	$\frac{BTU}{lbm}$	112.2	66.0
η_u	%	64.2	-
η_u*	%	-	48.6

OVER-ALL:

L_u	=	178.2	BTU/lbm
L_i	=	176	BTU/lbm
η_i*	=	56.7%	-
U/C_o	=	.133	-

	Nozzle	Rotor I	Rev. Vanes	Rotor II
Number of blades	43	98	97	94
Blading Efficiency	.91	.80	.83	.86
Blade Throat Area $in.^2$	111.5	141.5	184.5	227.5
Reaction (R_x)	.9	0	.03	.07

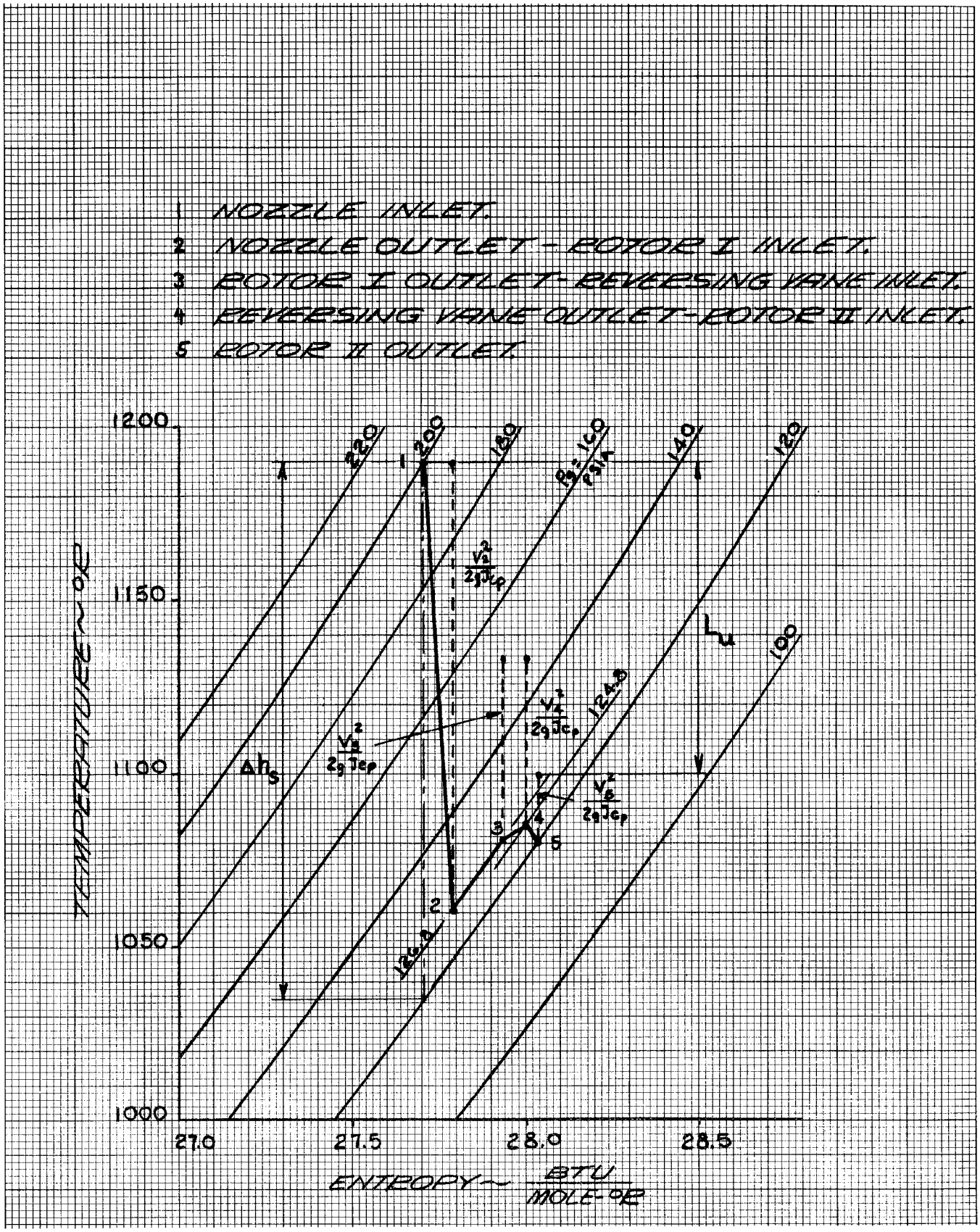

Figure 10. Expansion Process in T-S Chart

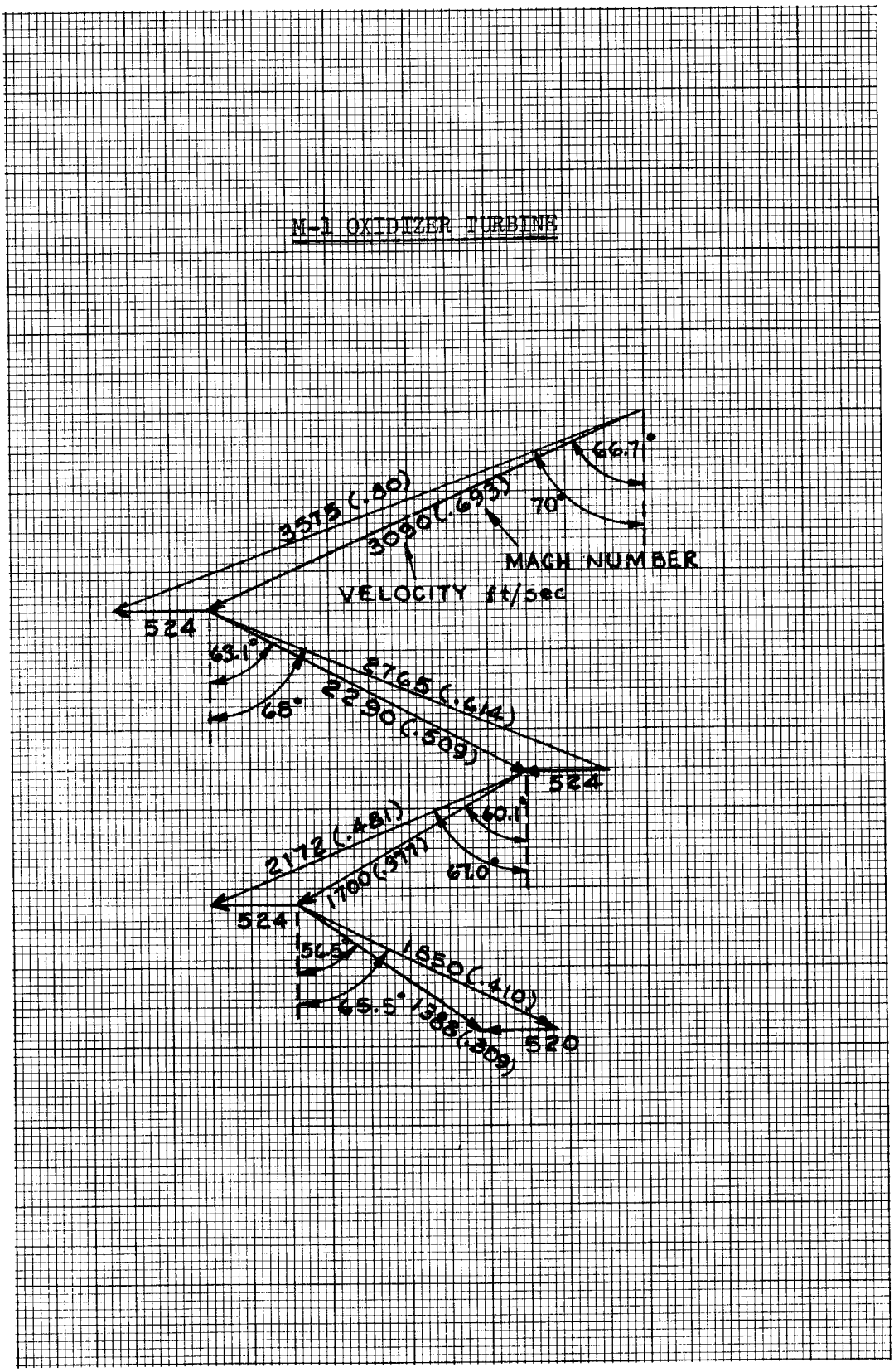

Figure 11. Velocity Triangles at the Mean Diameter

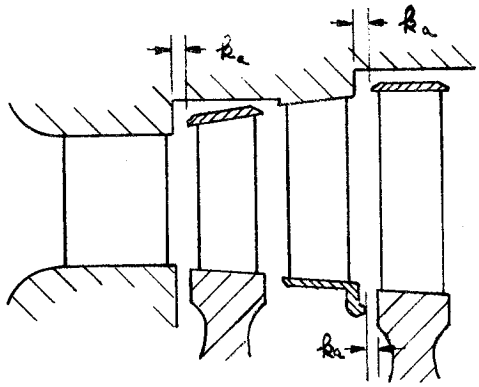

Figure 12. Seal Arrangement Assumed in Performance Calculations

TABLE 3

FLOW QUANTITIES AT HUB, MEAN, AND TIP
(Configuration slightly different than that finally selected)

		HUB					MEAN					TIP				
		Nozzle Inlet	Nozzle Outlet	Rotor I Outlet	Rev.Vane Outlet	Rotor II Outlet	Nozzle INLET	Nozzle Outlet	Rotor I Outlet	Rev.Vane Outlet	Rotor II Outlet	Nozzle INLET	Nozzle Outlet	Rotor I Outlet	Rev.Vane Outlet	Rotor II Outlet
D	in.	29.79	29.29	29.07	28.08	27.18	33.00	33.00	32.90	32.90	33.00	36.21	36.21	36.73	37.32	38.82
r	ft	1.240	1.240	1.210	1.170	1.132	1.375	1.375	1.370	1.370	1.375	1.510	1.510	1.530	1.570	1.618
P_T	psia	200.0	-	-	-	124.0	200.0	-	-	-	127.2	200.0	-	-	-	130.5
P_S	psia	200.0	115.5	119.2	115.0	115.0	200.0	126.8	126.8	124.8	120.0	200.0	136.0	132.2	132.2	124.4
T_T	°R	1190	1190	1133.8	1133.8	1102.5	1190	1190	1133.0	1133.0	1100.9	1190	1190	1132.4	1132.4	1100.3
T_s	°R	1190	1038	1067.8	1072.0	1080.8	1190	1061	1080.5	1086.4	1083.8	1190	1081	1088.6	1097.2	1086.7
ρ	lb/ft^3	-	.0380	.0382	.0367	.0364	-	.0407	.0401	.0393	.0380	-	.0429	.0415	.0412	.0391
V	ft/sec	-	3880	2560	2475	1445	-	3570	2299	2150	1300	-	3310	2080	1868	1162
U	ft/sec	-	472	461	445	431	-	524	522	522	524	-	575	582	598	615
W	ft/sec	-	3440	2980	2070	1850	-	3080	2770	1680	1760	-	2770	2615	1340	1695
α	°	0	70.0	-64.1	67.0	-59.1	0	70.0	-63.1	67.0	-56.6	0	70.0	-61.9	67.0	-53.5
β	°	-	67.3	-68.0	62.2	-66.0	-	66.7	-68.0	60.0	-66.0	-	65.9	-68.0	56.1	-66.0
$\rho V_x r$	$\frac{lbm}{ft.-sec.}$	-	63.0	51.5	41.4	31.0	-	68.2	57.1	45.2	37.4	-	73.1	62.2	48.3	43.6
rV_u	$ft.^2/sec.$	-	4525	-2780	2660	-1425	-	4620	-2810	2710	-1488	-	4700	-2810	2685	-1512

$\dot{m} = 2\pi \int_{r_h}^{r_t} \rho V_x r \, dr$

Nozzle Inlet	Nozzle Outlet	Rotor Outlet	Rev. Vane Outlet	Rotor II Outlet
-	115.2	115.0	113.8	114.5

$\dot{m} L_u = 2\pi w \int_{r_h}^{r_t} \rho V_x r \, \Delta(rV_u) \, dr$

Stage I	Stage II
12950	7290

General: HP = 1.415(12950 + 7290) = 28600 HP

The calculations above are based on the following blading efficiencies:

Nozzle	Rotor I	Rev. Vane	Rotor II
.91	.81	.81	.79

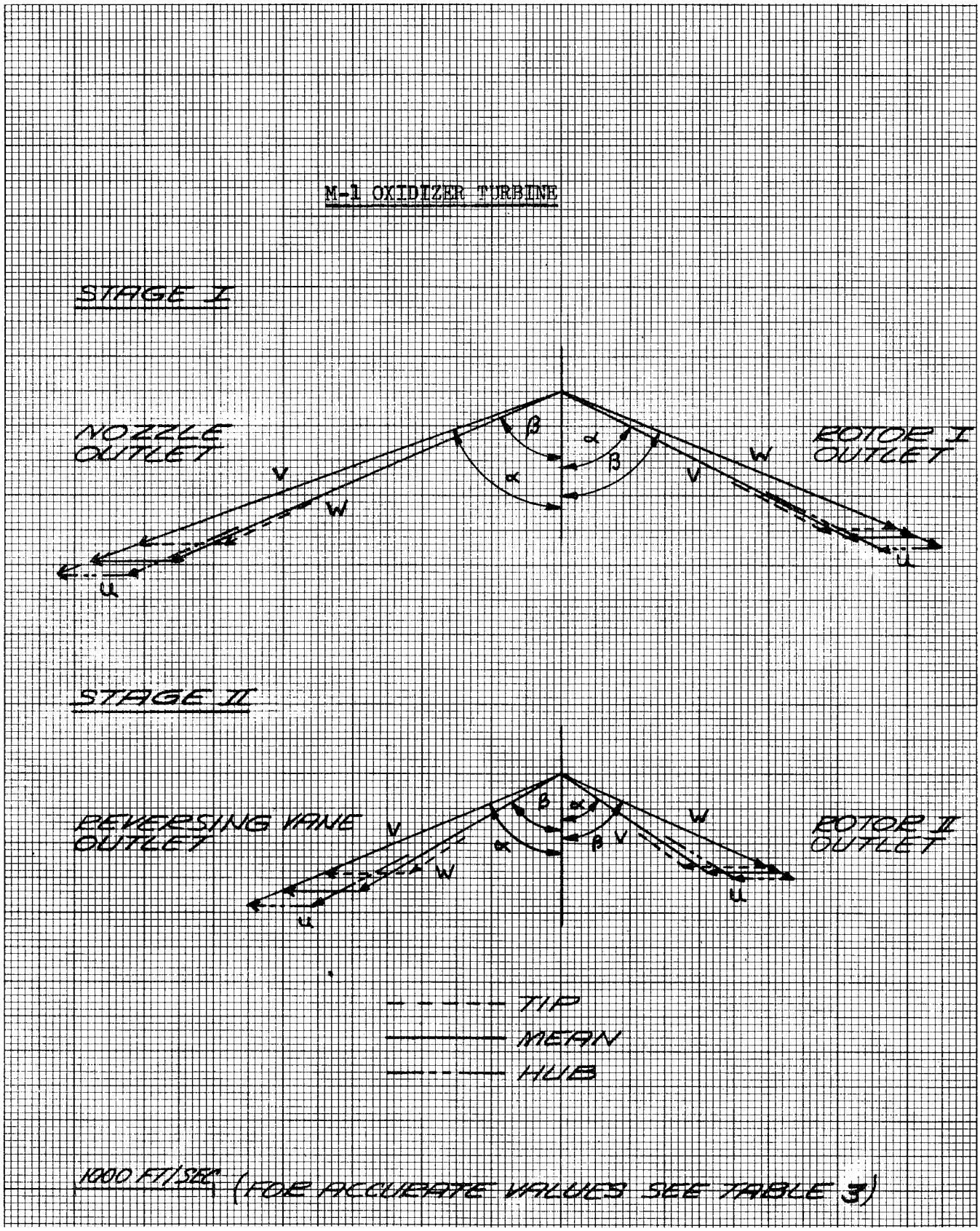

Figure 13. Velocity Triangles at Hub, Mean, and Tip

2. Blade Profiles

Figure 14 illustrates the profiles suggested by Loschge[8] and Traupel for impulse bladings with large turning angles. Further, Traupel indicates that the loss prediction of Appendix B is consistent with profiles of this general shape.

The velocity coefficients of two impulse blades are compared on Figure 15[9]. Blade B shown on Figure 15 (blunt leading edge) has a better design point and off-design performance than the classical Blade A.

The blunt profile is efficient over a large incidence range which guarantees good off-design performance. Possibly large pressure variations in the manifold which result in large variations of nozzle exit and rotor inlet velocities do not have a significant effect upon performance.

It appears that sharp leading edges should be avoided whenever possible in a turbine having a very fast start transient and operating in the combustion products of liquid hydrogen and oxygen. Under these conditions, extreme heat transfer rates to the blades have been known to cause cracking of the sharp leading edges.

Considering the small change in relative inlet and outlet angles between the low reaction blade rows (see Figure 11), it appears feasible to use the same profile for both rotors and the reversing vanes. Further, it can be noted from Figure 13 that there is a small variation in the gas inlet angles from the hub to the tip for all blade rows. Therefore, an untwisted profile of constant cross-section having the general shape shown on Figure 14 (Loschge) was selected for both rotors and the reversing vanes. The variation in blade outlet angles from first to second rotor is achieved by an appropriate decrease in stagger angles.

Because of the blunt leading edge, the axial distance between the stator outlet and the rotor inlet is necessarily large to permit the proper velocity distribution to be established at the blade nose.

The configuration of the inlet manifold was considered in selecting the nozzle profile. Because of the geometry of the turbine inlet manifold (2 inlets at 80° included angle), the inlet velocity is not axial in a large portion of the circumference; in fact both positive and negative incidence angles exist. The large leading edge radius and the pronounced contraction of the flow at the nozzle intake assure good performance at various incidence angles.

Figures 16 and 17 show the coordinates for the two basic profiles. Pitch, cord, and stagger angle at the mean diameter (33.00-in.) are shown on Figure 18 for all of the blade rows. Figure 19 shows the axial plan under hot conditions.

(8) Loschge, A., Konstruktionen aus dem Dampfturbinenbau, Springer Verlag/ Berlin/Gottingen/Heidelberg, 1955
(9) Loschge, A., op. cit., Figure 23

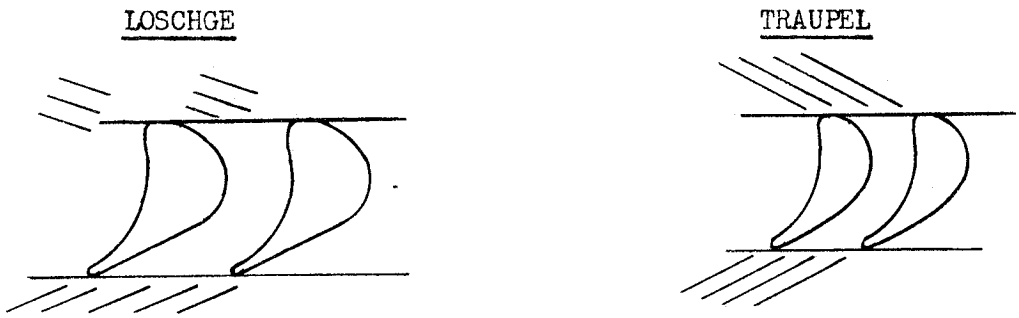

Figure 14. Impulse Profiles for Large Turning Angles

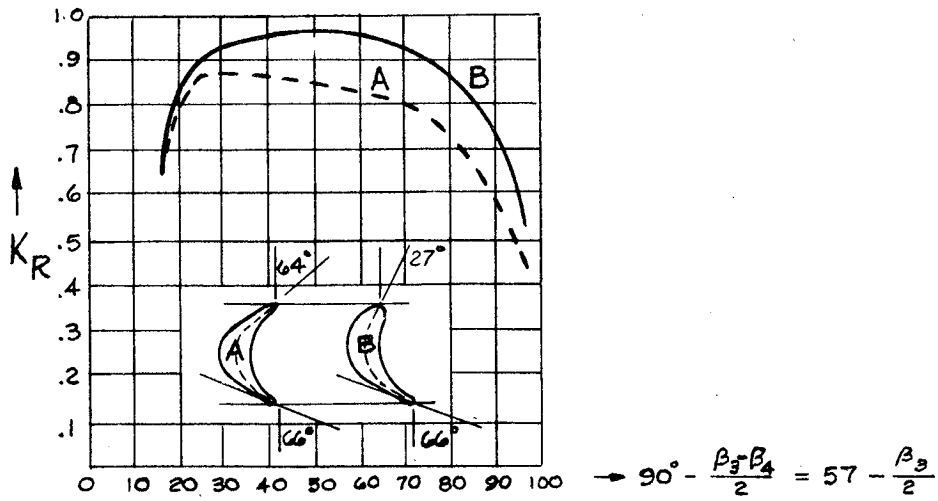

- ANGLES IN FIGURE REPRESENT BLADE MEANLINE ANGLES
- β_3 AND β_4 ARE ACTUAL GAS ANGLES
- β_3 = INLET, $\beta_4 = 66°$ = OUTLET)

Figure 15. Comparison of the Velocity Coefficients of Blades with Blunt and Sharp Leading Edges

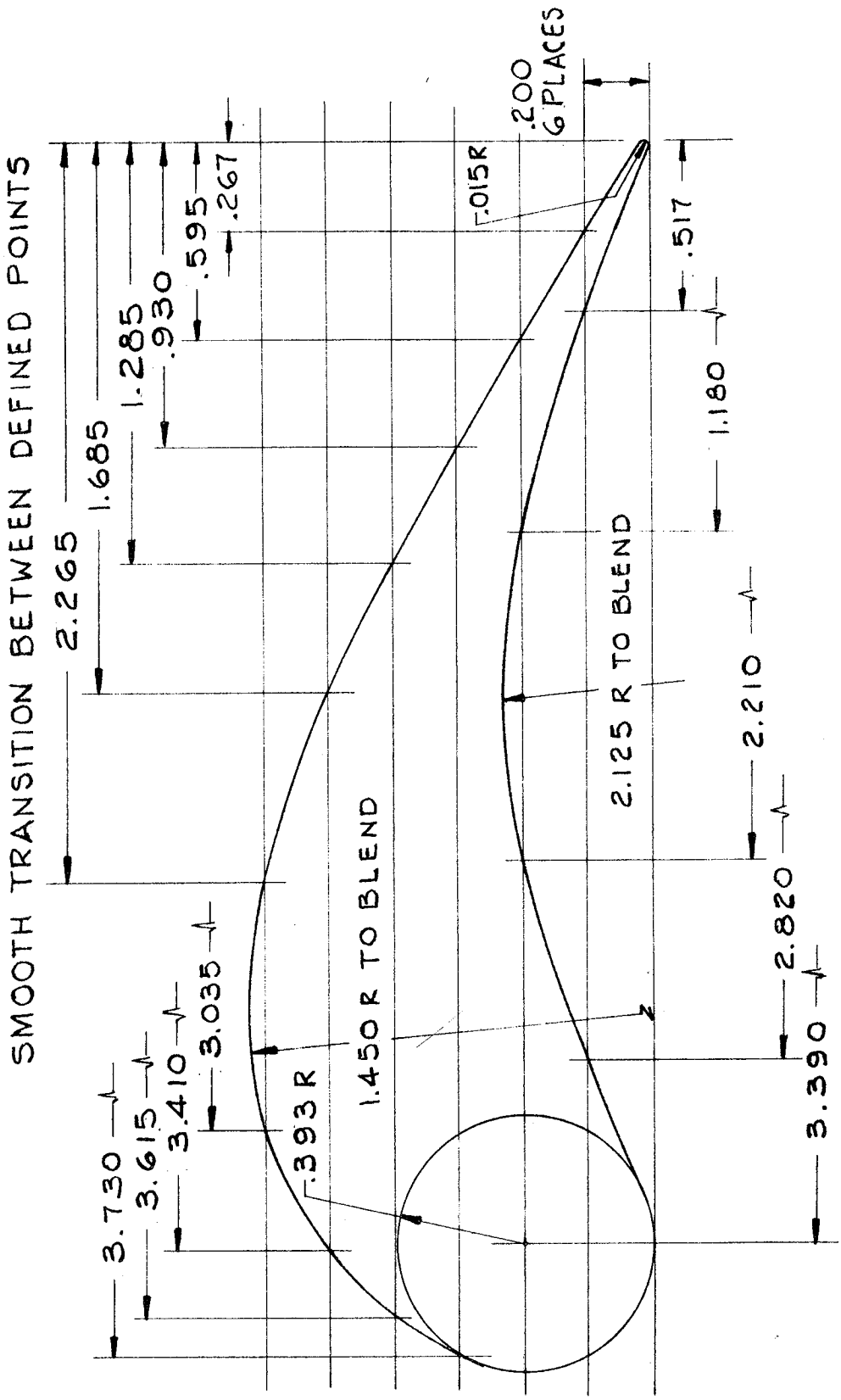

Figure 16. Nozzle Vane Profile and Coordinates

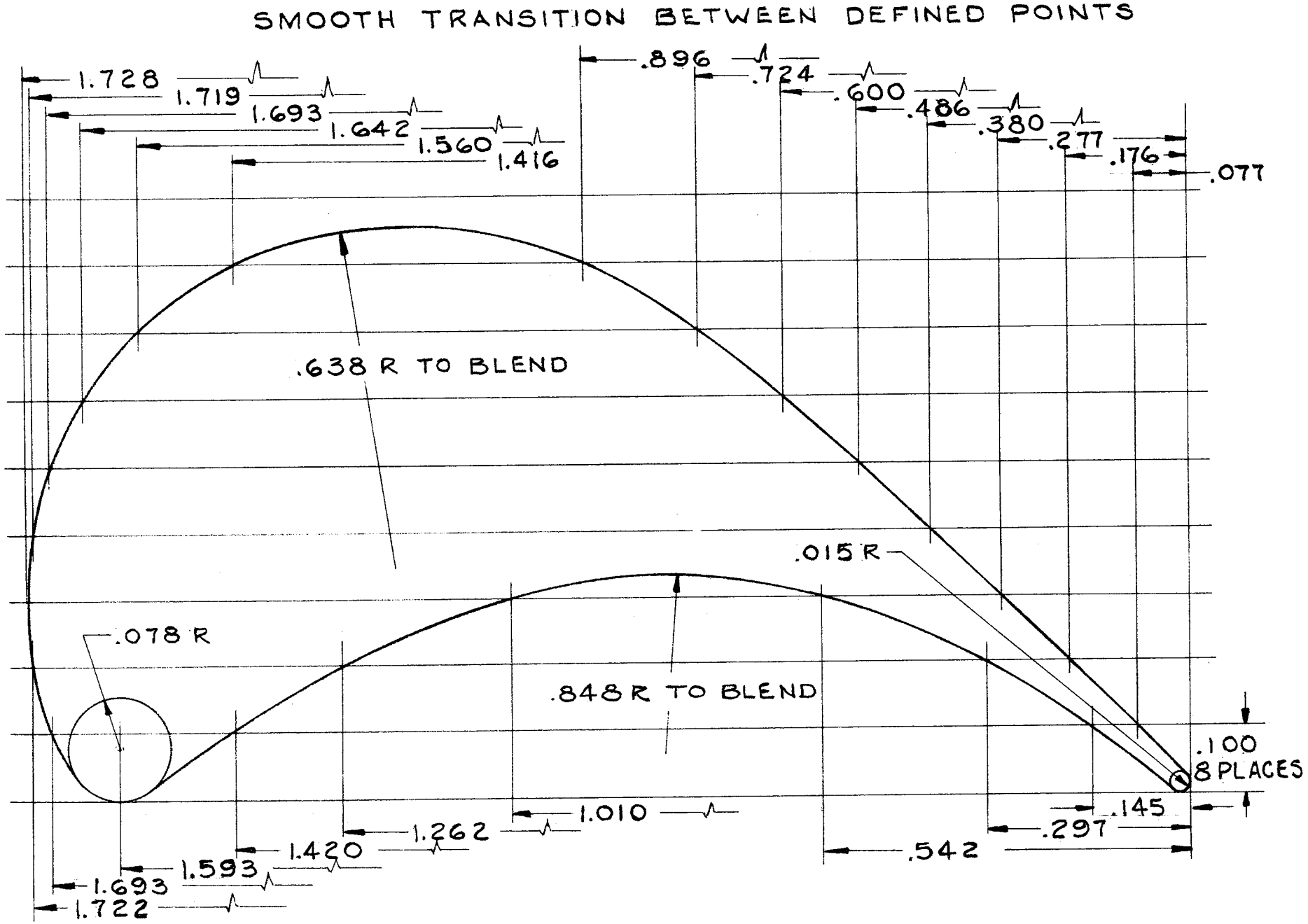

Figure 17. Rotor Blade Profile and Coordinates

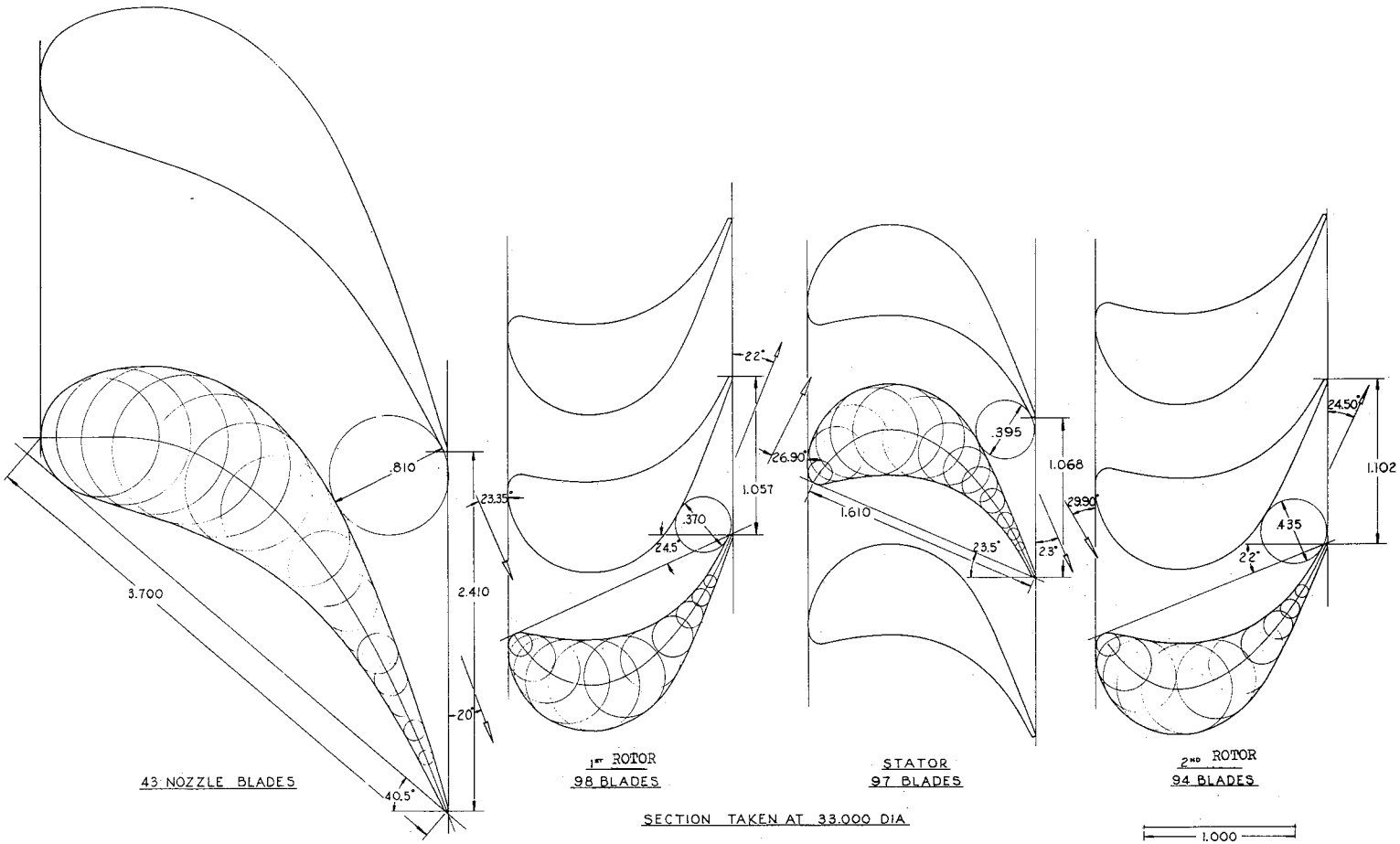

Figure 18. Blade Layout

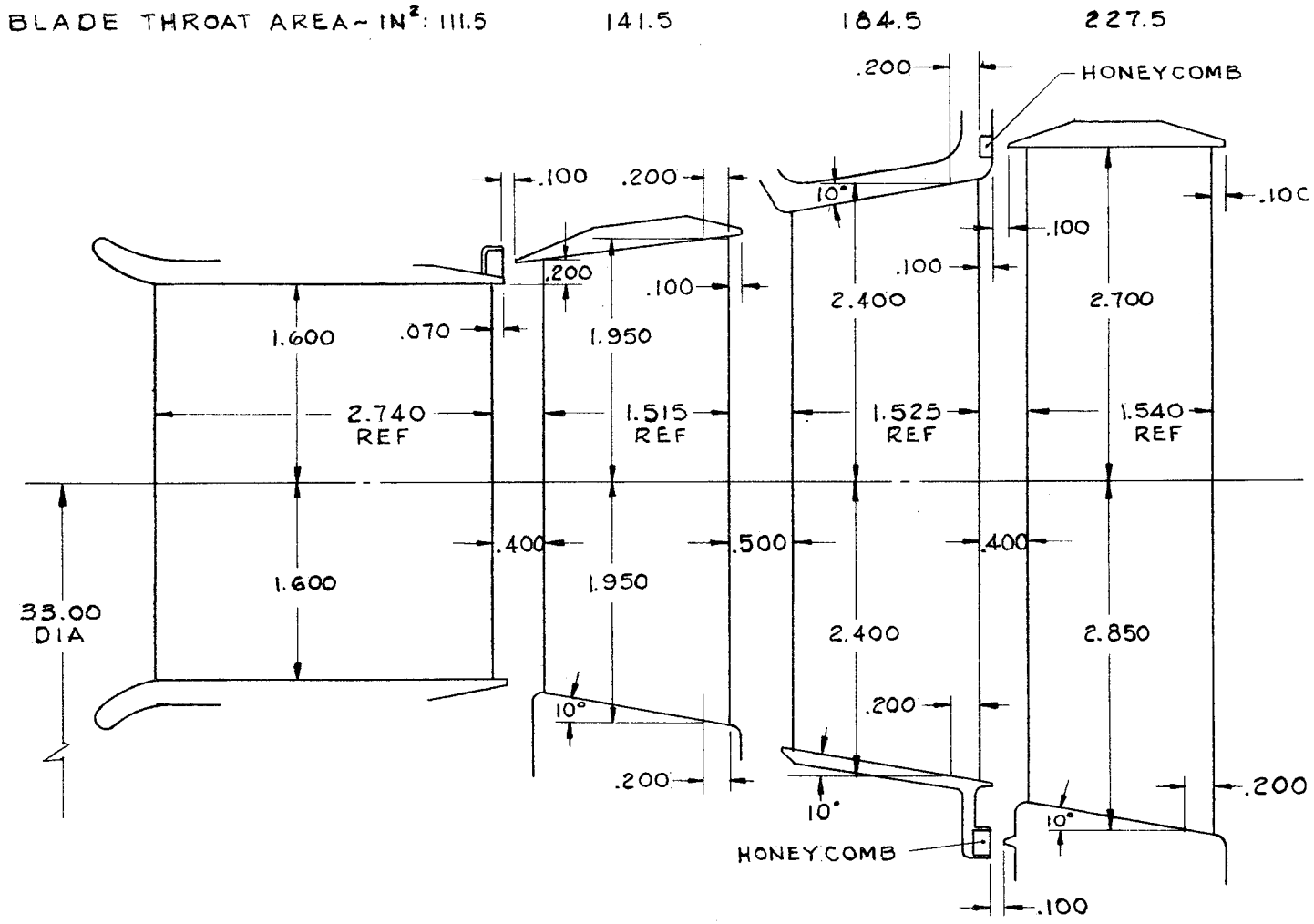

AXIAL PLAN, HOT CONDITIONS
CLEARANCES SHOWN FOR RUNNING CONDITIONS

Figure 19. Axial Plan in Hot Condition

3. Determination of Cascade Exit Angles

Four different methods were used to make an estimation of the gas outlet angle for an assumed blade row with the following results:

Method	Outlet Angle
Ainley[10]	67.3
Traupel[11]	66.3
Zappa[12]	65.0
Markov[13]	65.1

Because the tangential component of the velocity is responsible for the specific work of the stage, it is preferable to select one of the more conservative methods of Zappa or Markov. Zappa is the more convenient to use; therefore, it was selected for the current design. This method, illustrated on Figure 20, expresses the gas efflux angle of a blade row as a function of the ratios, throat width to pitch (d/s), and trailing edge thickness to pitch (te/s).

4. Flow Areas

The accurate determination of the flow areas is of the utmost importance for obtaining the required reaction distribution in the turbine. The performance calculations from the performance discussion (III, C, 1, b) give preliminary values of the required free stream blade height at the exit of the blade rows. These blade heights were corrected using Vavra's method[14]. The flow through a turbine blade row is expressed by the equation:

$$\frac{\dot{m}\sqrt{T_T}}{P_T} = \frac{A}{\sqrt{R/g_o}}\sqrt{\frac{2\gamma}{\gamma-1}}\sqrt{\left(\frac{P_s}{P_T}\right)^{2/n} - \left(\frac{P_s}{P_T}\right)^{\frac{n+1}{n}}}$$

(10) Ainley, D. G., op. cit.
(11) Traupel, Walter, op. cit.
(12) Zappa, O., Plot of Gas Efflux Angle from Turbine Blade Cascade (Private Communication) based upon: NACA TN 3802, 1956 (Dunavant, J. C. and Erwin, J. R., Investigation of a Related Series of Turbine Blade Profiles in Cascade) and NACA TN 3959, 1957 (Dunavant, J. C., Cascade Investigation of a Related Series of 6-Percent Thick Guide Vane Profiles and Design Charts)
(13) Markov, N. M., Calculation of the Aerodynamic Characteristics of Turbine Blading, Associated Technical Services Inc., Glen Ridge, New Jersey, 1958
(14) Vavra, M. H., op. cit.

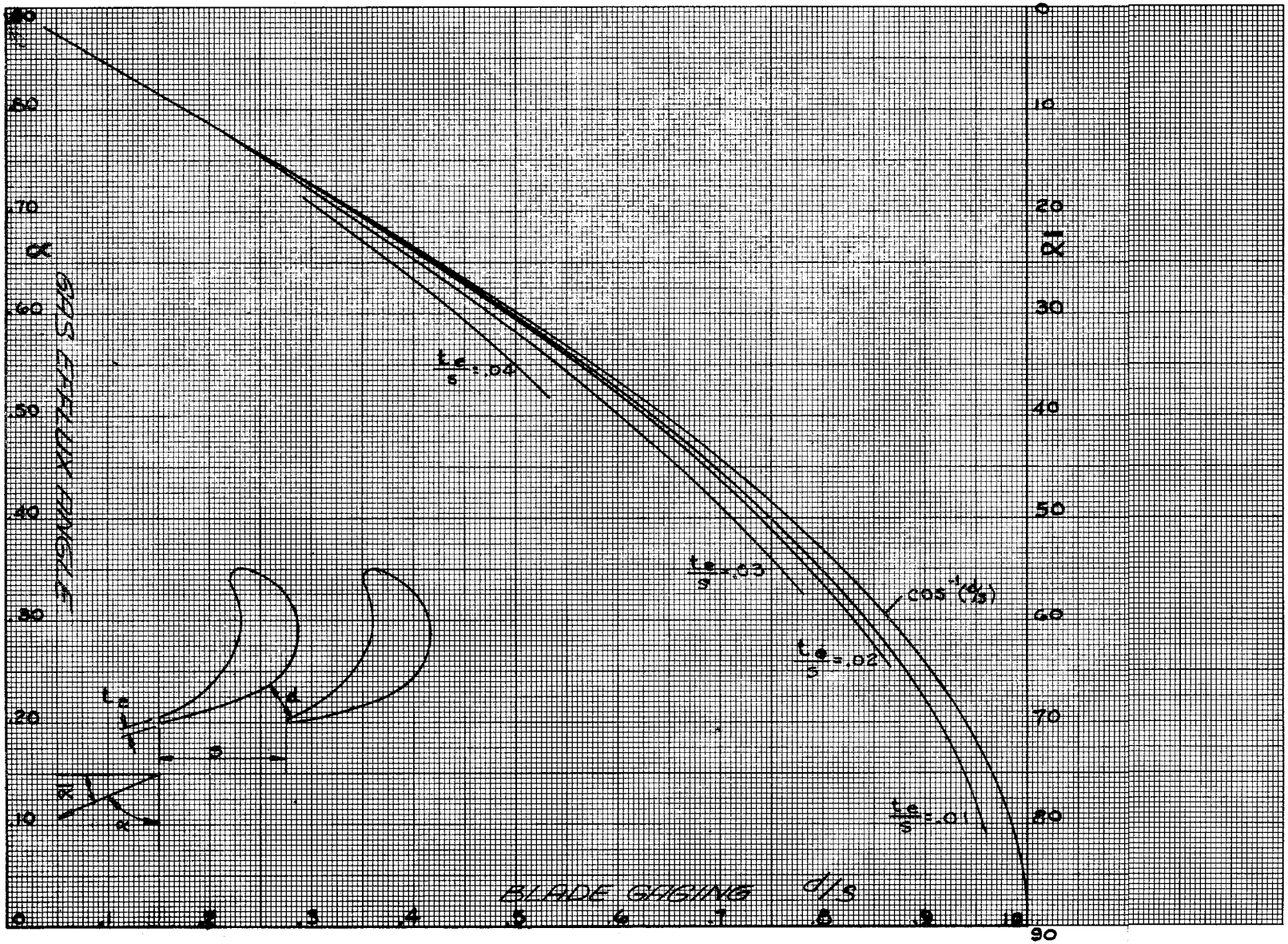

Figure 20. Gas Efflux Angle from Turbine Blade Cascade

with:

$$n = \frac{\gamma}{\gamma - \bar{\eta}_p (\gamma - 1)}$$

and: $\bar{\eta}_p = f$ (Pressure Ratio, Loss).

Different loss coefficients are used for calculating efficiency and flow areas. The mean polytropic efficiency, $\bar{\eta}_p$, for the calculation of the flow area is obtained from the blade efficiency with the following empirical relationship:

Nozzle: $\bar{\eta}_p = 1 - .50 (1 - \eta_n)$

Rotors and Reversing Vanes: $\bar{\eta}_p = 1 - .67 (1 - \eta_r)$

Table 4 shows the results of these calculations and presents a comparison of the blade heights obtained with those discussed under performance (III, C, 1, b). The above equations give the blade height at the blade throat while those in the performances discussion give the free stream annulus heights.

5. Velocity Distribution on Profiles

The following two methods were used to estimate the velocity distributions on the profiles.

a. NASA Computer Program(15)

The accuracy of the results obtained with this method depends to a large extent upon the accuracy with which the computer input is prepared. It proved difficult to estimate the effective channel at the inlet to the blades and as a result, the first points on the suction side outside of the physical channel were neglected in determining the diffusion parameter. Figure 21 is an example of the preparation of the computer input for the first rotor.

b. Vavra Potential Flow Method (16)

This method yields the inlet stagnation point and velocity distribution for any inlet angle. Its limitations are the inherent two-dimensionality of the field plotter and its restriction to incompressible flow.

---

(15) Stinson, W. D., Turbine Computer Program, NASA-Aerojet Computer Job No. 1009, Aerojet-General Corp. Memorandum dated 27 September 1962

(16) Vavra, M. H., Aero-Thermodynamics and Flow in Turbomachines, John Wiley & Sons, Inc., New York/London, 1960

TABLE 4

DETERMINATION OF THROAT AREAS AND BLADE HEIGHTS

		Nozzle	1st Rotor	Rev. Vanes	2nd Rotor
η	-	.91	.80	.83	.86
$\bar{\eta}_p$	-	.955	.867	.887	.907
n	-	1.361	1.315	1.324	1.335
P_T	psia	200	174.5	151.2	137.5
T_T	°R	1190	1157.5	1133.9	1114.7
P_S/P_T	-	.634	.727	.825	.873
$\mathring{m}/A_d$	$\frac{\text{lbm}}{\text{sec-in.}^2}$	1.039	.810	.621	.5025
k		1	1.0055	1.0030	1.0085
$A_d = \frac{\mathring{m}}{k} \frac{1}{\mathring{m}/A_d}$	in.^2	111	141.5	184.8	227.0
h_d	in.	3.19	3.90	4.82	5.55
h*	in.	3.20	3.83	4.78	5.46
h_d**	in.	3.20	3.90	4.80	5.55

* Appendix B Method (reference performance discussion, Section III, c, 1, b)

** Final Selection

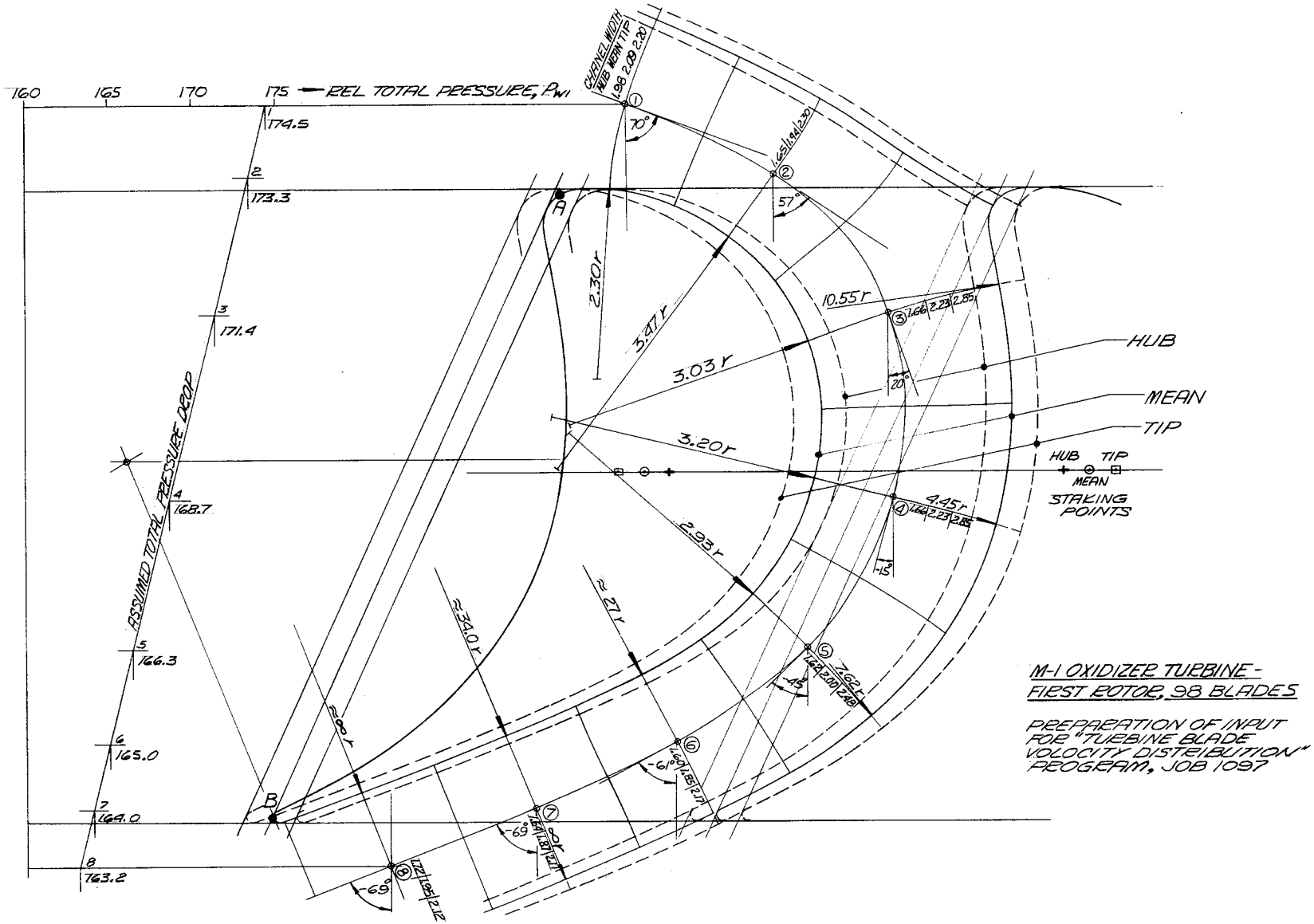

Figure 21. Example of the Preparation of the Computer Input for the First Rotor

Results from the velocity distribution analysis are as follows:

The ratio of the surface velocity to the outlet velocity is plotted in relationship to the distance measured along the blade surfaces from an aribtrary point, A (see Figure 21) (A is not the stagnation point). Because the Vavra method yields the inlet stagnation point, it is shown for the nozzle and the first rotor. The remaining two rows of blades were not investigated using the potential flow method; therefore, the velocity at A was assumed to be equal to the inlet velocity.

The stagnation point on the trailing edge, B, exists only in potential flow. Actually, the flow will separate; therefore, this stagnation point is not shown. Instead it is assumed that the trailing edge surface velocities at the pressure and suction sides are equal to the leaving velocity downstream from the blade row.

Two criteria were used to judge the velocity distribution:

Diffusion Parameter D
Kofskey[17] defines a diffusion

parameter as follows:

$$D = D_s + D_p$$

where:

$$D_s = 1 - \frac{W_4}{W_s \text{ max.}}$$

$$D_p = 1 - \frac{W_p \text{ min.}}{W_3}$$

A desirable value for D is .45. It is thought that the suction side contributes the major part of the total losses. Therefore, diffusion parameters larger than .45 were accepted providing D_s was smaller than approximately .25.

---

(17) Kofskey, M. G., Cold-Air Performance Evaluation of a Three-Stage Turbine having a Blade-Jet Speed Ratio of .156 Designed for a 100,000-Pound-Thrust Hydrogen-Oxygen Rocket Turbopump Application, TM-X-477, NASA Lewis Research Center, Cleveland, Ohio

Separation Parameter P

Vavra[18] defines a separation parameter as follows:

$$P = \frac{dS/d\xi \cdot |\xi|^{.8}}{(W/W_4)\ 2.2}$$

with

$$S = 1 - \left(\frac{W}{W_4}\right)^2$$

and $\xi = \ell/c$

and indicates that no separation will occur as long as:

$$P \leq .090 \ (Re_{c4})^{.2}$$

The separation parameter indicates that larger decelerations of the blade surface velocity are acceptable at the inlet to the blade than close to the trailing edge. This condition seems valid because the boundary layer builds up gradually along the blade surface. Apparently, a triangular velocity distribution, which has the maximum surface velocities near the leading edge, is optimum for the low reaction (rotor and reversing row) blades.

Figure 22 (a) shows the velocity distribution obtained for the nozzle at the design inlet angle while Figure 22 (b) compares the velocity distribution of the design inlet angle with off-design conditions for incidence angles of i = ± 30-degrees. Figure 22 indicates favorable velocity distributions; the selected profile seems adequate.

The velocity distribution of the first rotor blades at the design point conditions are shown on Figure 23 (a), which illustrates the attempted triangular distribution. The values of the separation parameter are acceptable (see Figure 23 (c)). The diffusion parameter on the suction side (D_s) is good. (Note that the first two stations, which are outside of the physically-defined channel are neglected in the calculation of D_s.) The diffusion parameter on the pressure side is large; however, it is thought that the pressure side contributes only a minor portion to the total loss. Figures 23 (b) and 23 (c) are a comparison between the velocity distribution and the separation parameter obtained for the design point inlet angle with the same parameters for incidence angles of +4 degrees and -7 degrees. The off-design performance of the blade seems satisfactory.

---

(18) Vavra, M. H., Private Communication

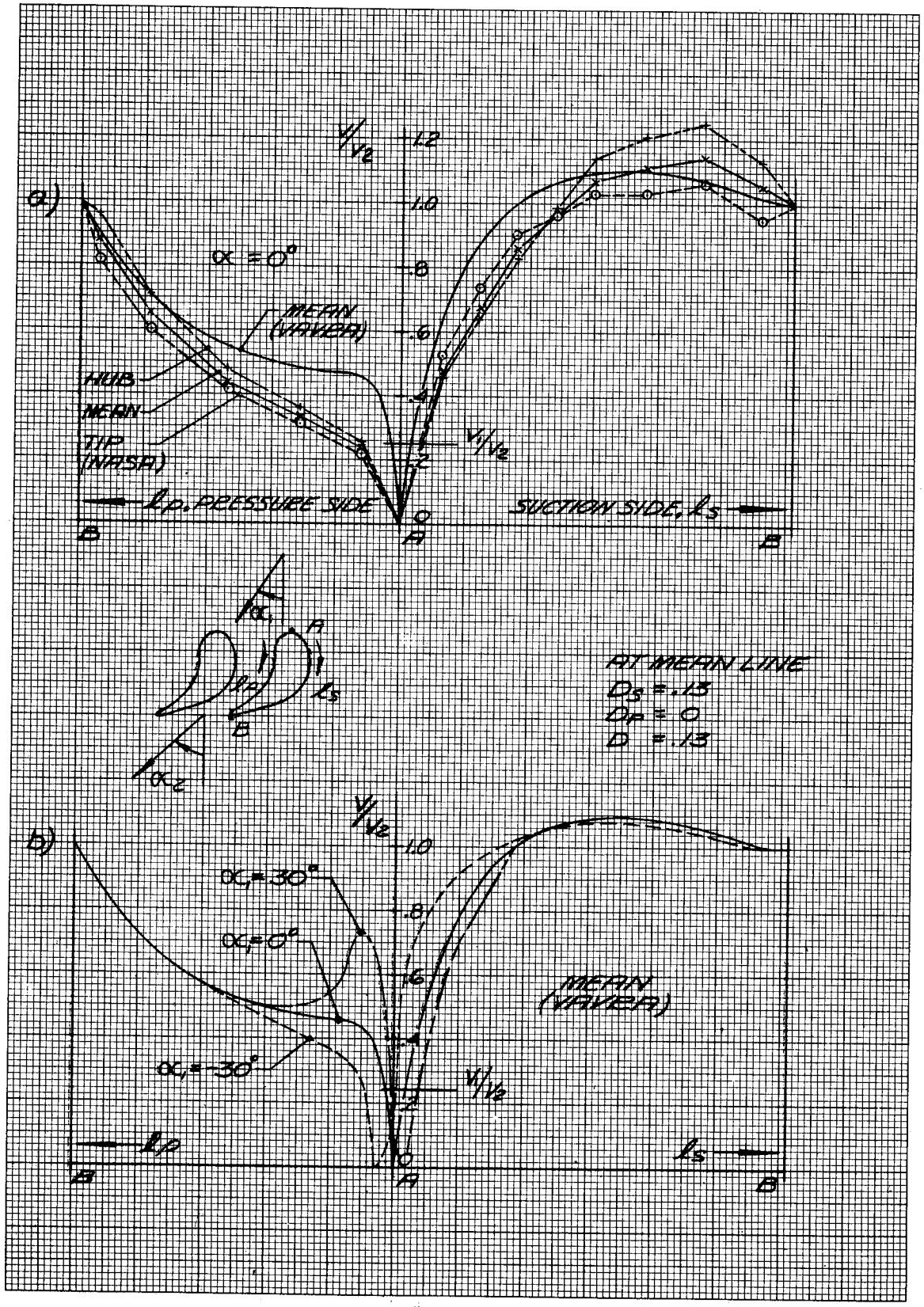

Figure 22. Velocity Distribution for Nozzle, 43 Vanes

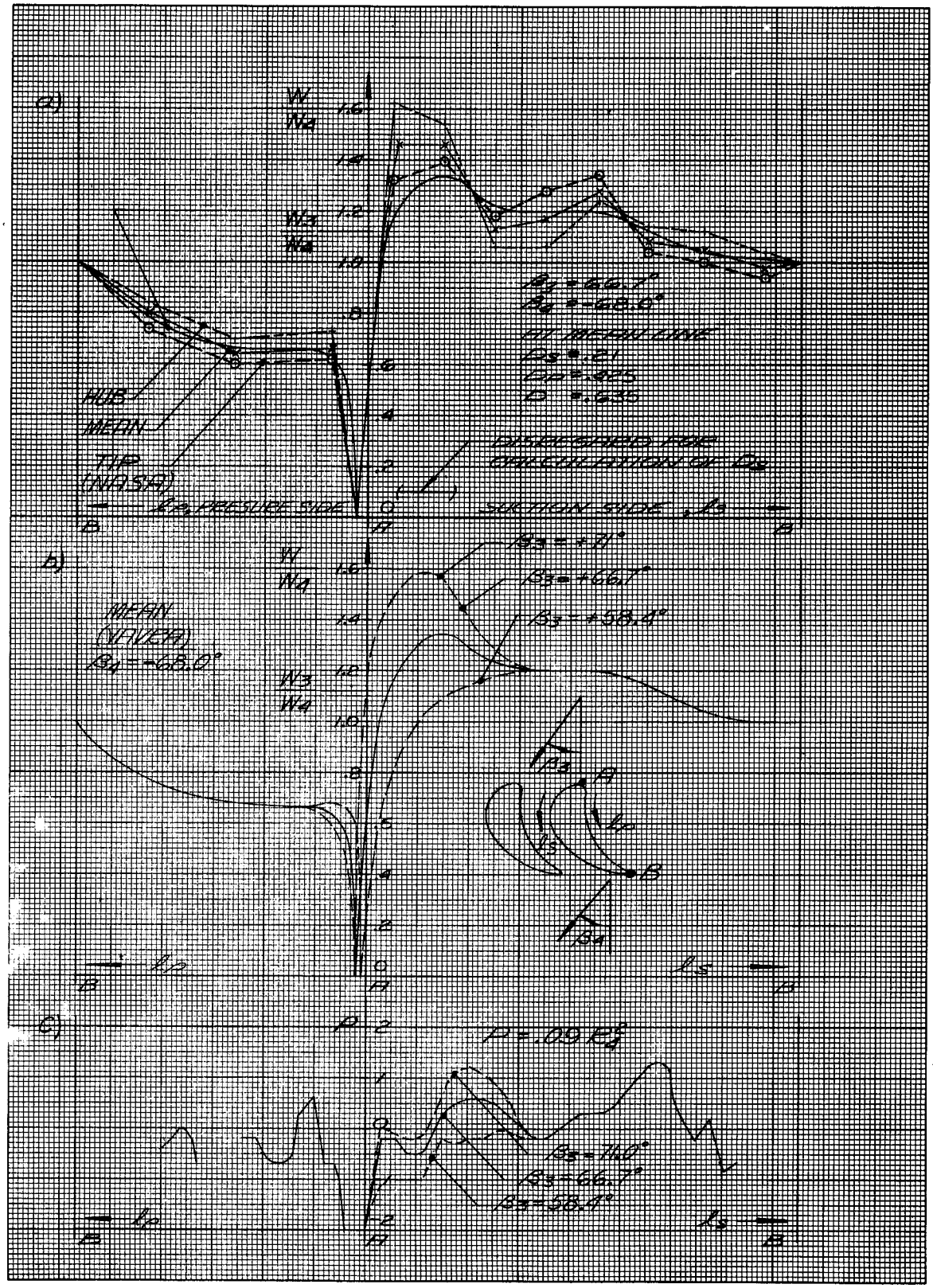

Figure 23. Velocity Distribution and Separation Parameter for First Rotor, 98 Blades

The velocity distribution for β_3 = 71-degrees in Figure 23 (b) (Method Vavra) closely resembles the one at the hub of Figure 23 (a) (Method NASA). The acceptable separation parameters for the velocity distribution of Figure 23 (b) β_3 = 71, indicates that velocity distributions according to Figure 23 (a) are acceptable even if the first two points were not neglected.

The velocity distributions for the reversing vanes (93 blades) and second rotor blades (88 blades) are shown on Figures 24 and 25, respectively. Again, the total diffusion factor is somewhat high because of a large contribution from the pressure side. The suction side is satisfactory and the profiles seem adequate.

For the second rotor, the effect of the solidity upon the velocity distribution was investigated for 98, 88, and 82 blades (see Figure 26).

The originally selected solidity (88 blades) proved to be too low; therefore, the number of blades for the reversing row and the second rotor was increased to 97 and 94 blades, respectively.

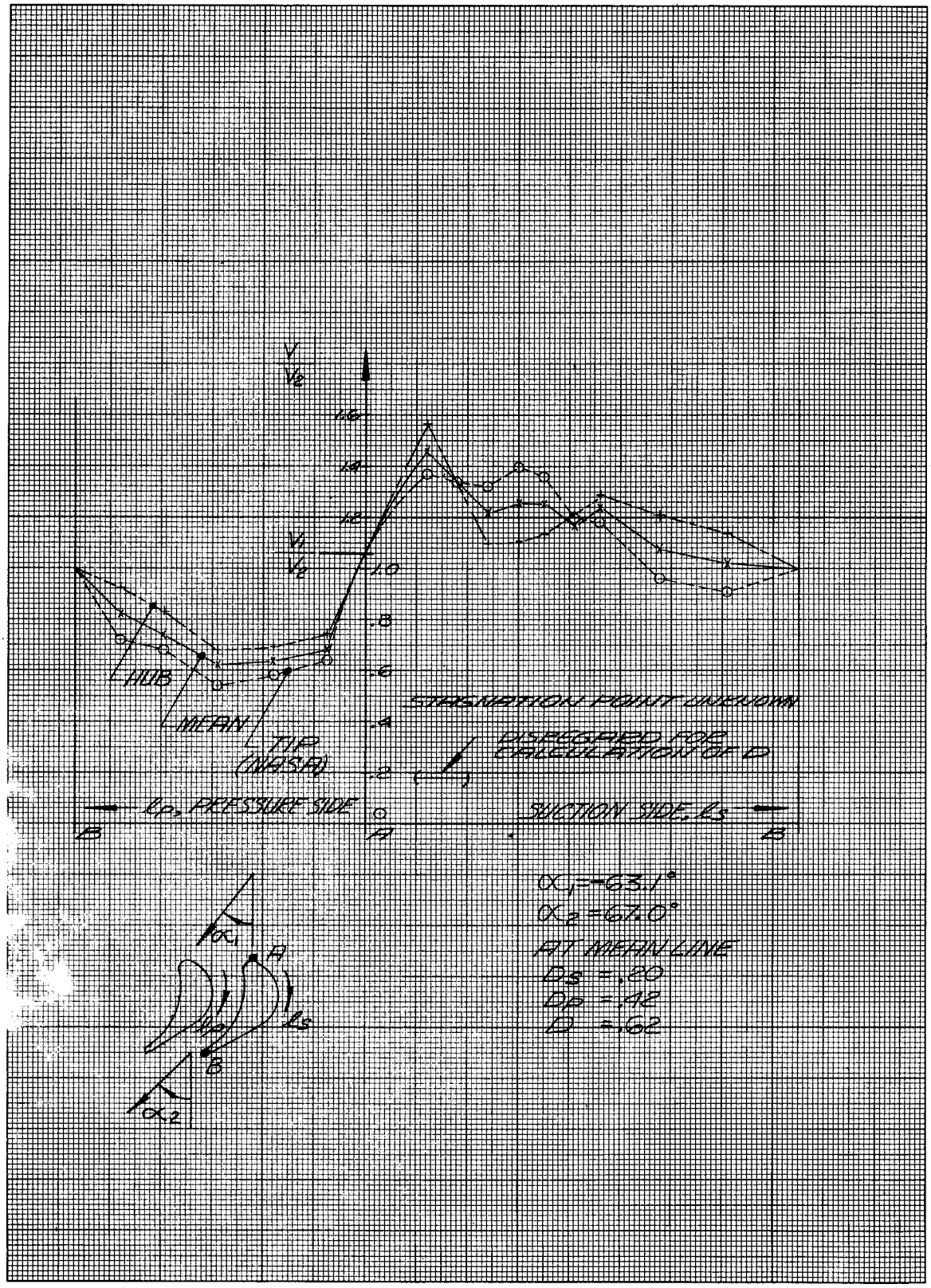

Figure 24. Velocity Distribution for Reversing Vanes, 93 Blades

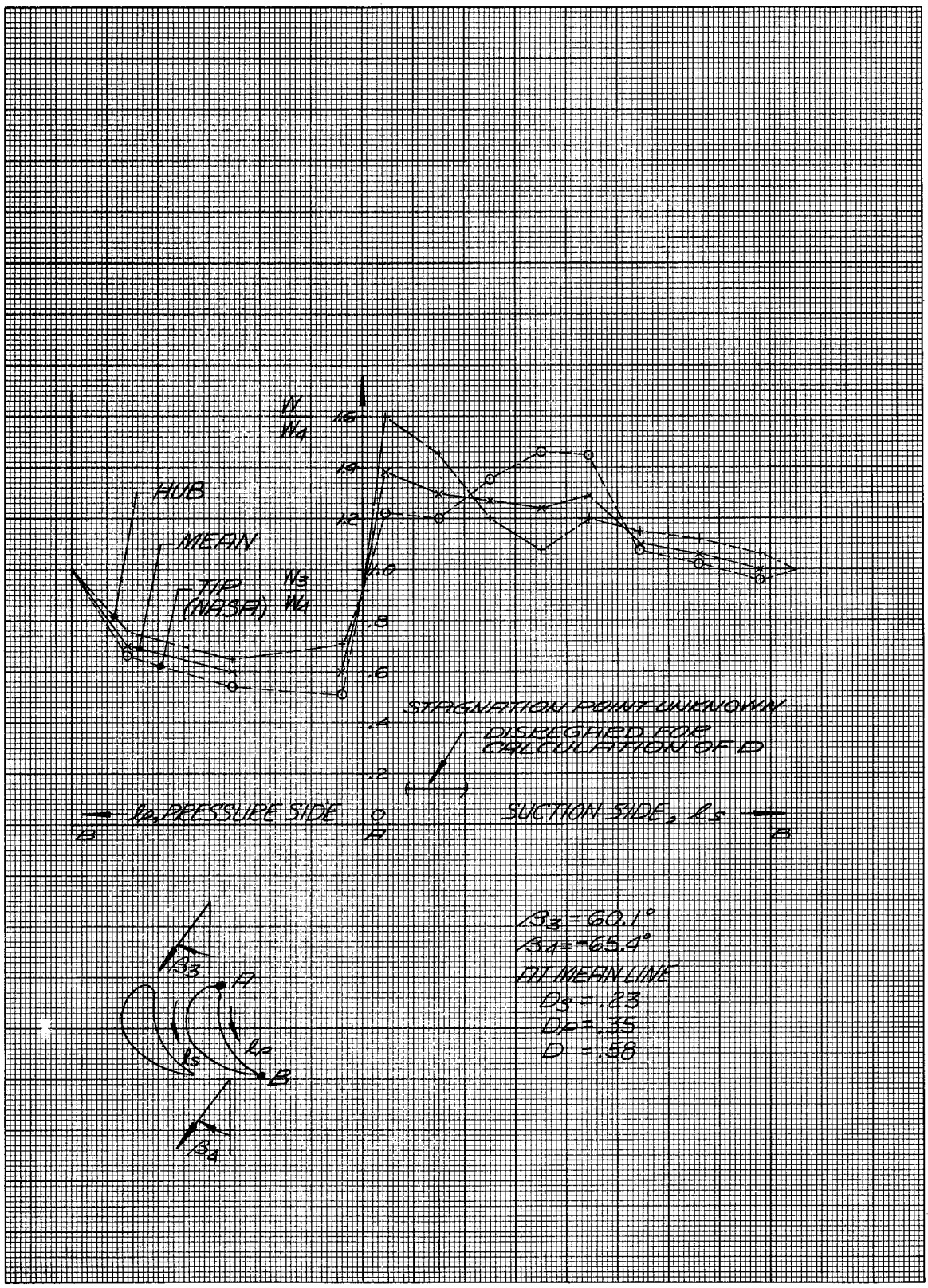

Figure 25. Velocity Distribution for Second Rotor, 88 Blades

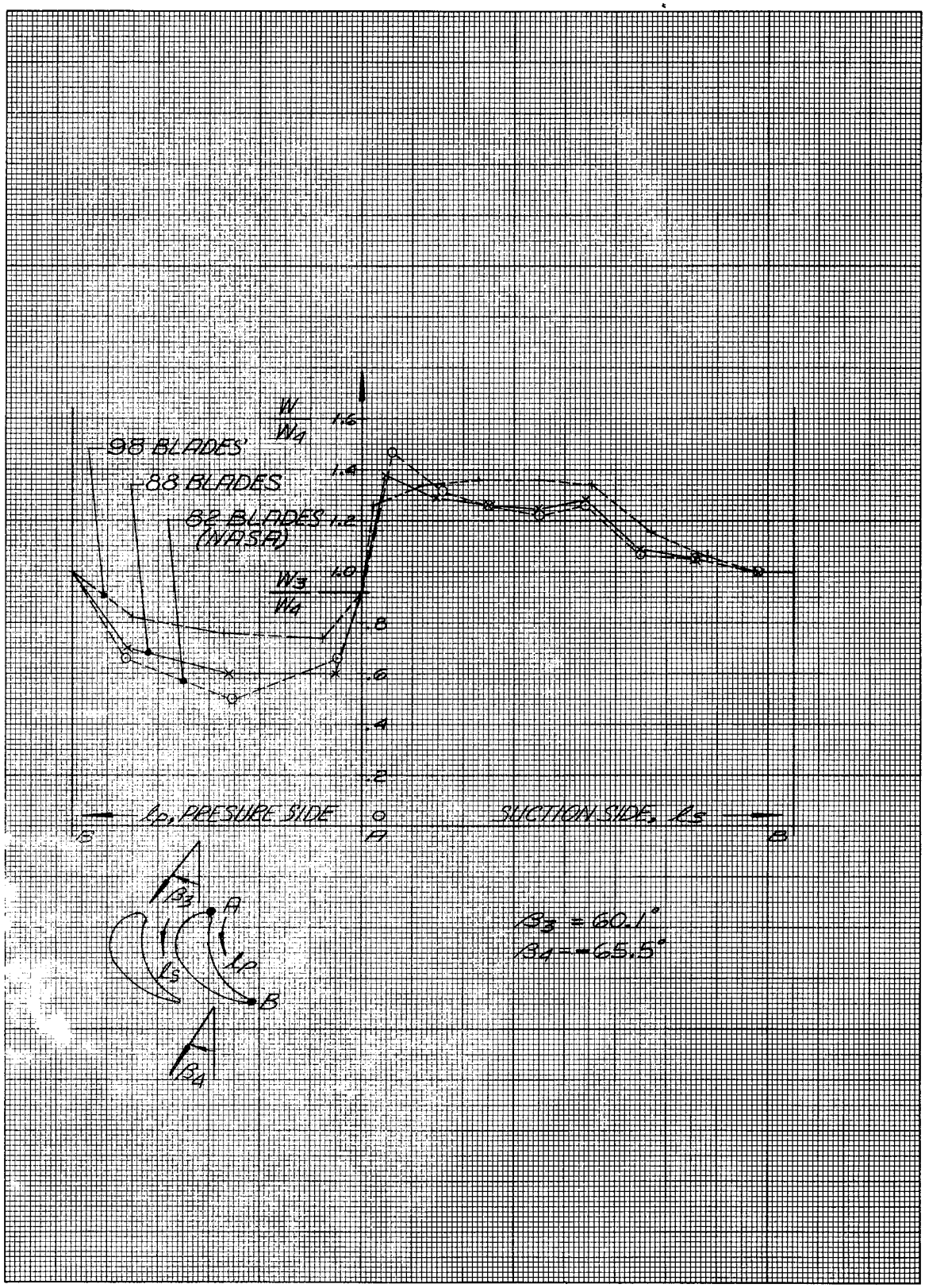

Figure 26. Velocity Distribution for Second Rotor, Comparison of 82, 88, and 98 Blades

BIBLIOGRAPHY

1. Ainley, D. G. and Mathieson, G. C. R., A Method of Performance Estimation for Axial-Flow Turbines, R&M 2974, December 1951

2. Flugel, Gustav, Die Dampfturbinen, ihre Berechnung und Konstruktion mit einem Anhang uber die Gasturbinen, Johann Ambrosius Barth, Leipzig, 1931

3. Kofskey, M. G., Cold-Air Performance Evaluation of a Three-Stage Turbine having a Blade-Jet Speed Ratio of .156 Designed for a 100,000-Pound-Thrust Hydrogen-Oxygen Rocket Turbopump Application, TM-X-477, NASA Lewis Research Center, Cleveland, Ohio

4. Loschge, A., Konstruktionen aus dem Dampfturbinenbau, Springer Verlag, Berlin/Gottingen/Heidelberg, 1955

5. Markov, N. M., Calculation of the Aerodynamic Characteristics of Turbine Blading, Associated Technical Services Inc., Glen Ridge, New Jersey, 1958

6. Stenning, Alan H., Design of Turbines for High-Energy-Fuel-Low-Power-Output Applications, MIT Report No. 79

7. Stinson, W. D., Turbine Computer Program, NASA-Aerojet Computer Job No. 1009, Aerojet-General Memorandum, 27 September 1962

8. Traupel, Walter, Thermische Turbomaschinen, Erster Band, Springer Verlag, Berlin/Gottingen/Heidelberg, 1958

9. Vavra, M. H., Analysis and Design of Modified 87-5 Turbine, AGLR #3, April 1962.

10. Vavra, M. H., Aero-Thermodynamics and Flow in Turbomachines, John Wiley & Sons Inc., New York/London, 1960

12. Zappa, O., Plot of Gas Efflux Angle from Turbine Blade Cascade (Private Communication) based upon:

    Dunavant, J. C. and Erwin, J. R., Investigation of a Related Series of Turbine Blade Profiles in Cascade, NACA TN 3802, 1956

    Dunavant, J. C., Cascade Investigation of a Related Series of 6-Percent Thick Guide Vane Profiles and Design Charts, NACA TN 3959, 1957

APPENDICES

APPENDIX A

-

NOMENCIATURE

a	Local Speed of Sound $a^2 = \gamma g_o R T_s$	ft/sec
a*	Critical Speed of Sound $a^{*2} = \frac{2\gamma}{\gamma+1} g_o R T_T$	ft/sec
A	Area	in^2
b	Axial Blade Width	inch
Δb	Axial Distance Between Blade Rows	inch
c	Blade Chord	inch
C_o	Isentropic Velocity $C_o^2 = 2g_o J \Delta H'$	ft/sec
c_p	Specific Heat at Constant Pressure	BTU/lb-°R
c_v	Specific Heat at Constant Volume	BTU/lb-°R
d	Throat Width	inch
D	Diameter	inch
D	Diffusion Parameter	---
D_S	Diffusion Parameter of Suction Side	---
D_P	Diffusion Parameter of Pressure Side	---
g_o	Proportionality Factor in Newton Second Law 32.17	$\frac{\text{lbm-ft}}{\text{lbf-sec}^2}$
h	Blade Height	inch
h	Specific Static Enthalpy	BTU/lb
i	Incidence	degree
J	Mechanical Equivalent of Heat (778.2)	ft lb/BTU
K_R	Rotor Velocity Coefficient W_4/W_4'	---
k_a	Axial Clearance	inch
k_r	Radial Clearance	inch
$K_{s/c}$	Relative Roughness	---
k	Leakage Factor	---
k	Thermal Conductivity	$\frac{\text{BTU}}{(\text{ft-HR-°R})}$

ℓ_s	Length of Point on Blade Surface from Point A on Suction Side	inch
ℓ_p	Length of Point on Blade Surface from Point A on Pressure Side	inch
L_u	Specific Work in Blading	$BTU/_{LBm}$
L_i	Specific Internal Work	$BTU/_{LBm}$
M	Absolute Mach Number	---
M	Molecular Weight	---
M_R	Mach Number Relative to Rotor Blade	---
$\dot{m}$	Mass Flow	lbm/sec
n	Number of Blades in a Row	---
n	Polytropic Exponent	---
N	Rotational Speed	rpm
$O/_F$	Mass Ratio Oxidizer/Fuel	---
P	Separation Parameter	
P_s	Static Pressure	psia
P_T	Total Pressure	psia
P_{TR}	Total Pressure Relative to Rotor Blade	psia
Pr	Prandtl-Number	---
q	Dynamic Head $\frac{1}{2}\frac{\rho V^2}{g_o 144}$	psi
R	Gas Constant	$\frac{\text{lbf-ft}}{\text{lbm-}^\circ\text{R}}$
r	Radius	ft
Re	Reynolds Number	---
Re_c	Reynolds Number based on Blade Chord	---
Re_{Dh}	Reynolds Number based on Hydraulic Diameter	---
R_x	Degree of Reaction: $R_x = \frac{T_{s2}' - T_{s4}'}{T_{T1} - T_{s4}'}$	---
s	Blade Pitch	inch

t		Maximum Blade Thickness	inch
t_e		Trailing Edge Thickness	inch
T_B		Effective Blade Temperature	°R
T_T		Total Temperature	°R
T_s		Static Temperature	°R
T_{TR}		Total Temperature Relative to Rotor Blade	°R
U		Wheel Velocity	ft/sec
V		Absolute Velocity	ft/sec
W		Velocity Relative to Rotor	ft/sec
α	(alpha)	Angle Between Axial Direction and Absolute Gas Velocity	degrees
β	(beta)	Angle Between Axial Direction and Relative Gas Velocity	degrees
γ	(gamma)	$\gamma = \frac{c_p}{c_v}$	---
δ	(delta)	Deviation	degrees
Δ	(delta)	Prefix to Indicate Change	---
ζ	(zeta)	Loss Coefficient	---
η_u		Blading Efficiency, total to total	---
η^*_u		Blading Efficiency, total to static	---
η_i		Internal Efficiency, total to total	---
η^*_i		Internal Efficiency, total to static	---
η_T	(eta)	Turbine Efficiency Based on Total to Static Pressure Ratio	---
$\bar{\eta}_p$		Mean Politropic Efficiency	---
η_n		Flow Efficiency in Nozzle Blading	---
η_r		Flow Efficiency in Rotor Blading	---
Z	(zeta)	Stagger Angle	degrees

θ	(theta)	Camber Angle	degrees
μ	(mu)	Absolute Viscosity	$LBm/_{(HR\text{-}ft)}$
ρ	(rho)	Density	lbm/ft^3
σ	(sigma)	Blade Solidity = c/s	---

SUBSCRIPTS

1	Inlet Stator
2	Outlet Stator
3	Inlet Rotor
4	Outlet Rotor
d	At Blade Throat
h	At Blade Root
m	At Mean Blade Height
t	At Blade Tip
u	Tangential Component
x	Axial Component

Subscript preceding a symbol indicates the number of the stage.

SUPERSCRIPT

'	Attached to temperature or enthalpy means value for isentropic expansion.

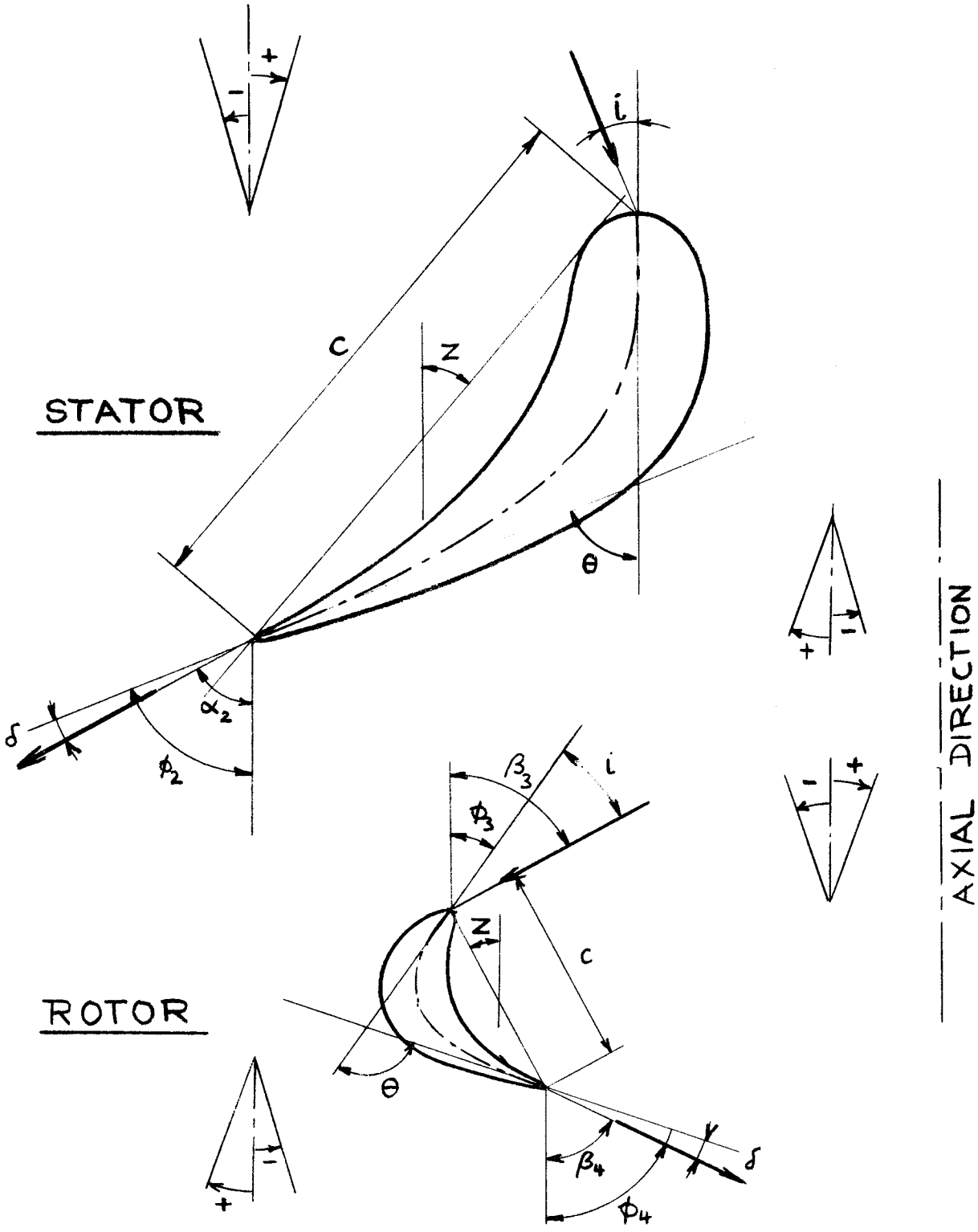

BLADE NOMENCLATURE AND SIGN CONVENTION

APPENDIX B

ESTIMATING LOSSES IN A TURBINE STAGE

Traupel[1] presents a complete and consistent system for estimating losses in a turbine stage. Because this loss system was used for the M-1 oxidizer turbine design, the pertinent portion of Chapter 8.4[1] is abstracted and presented herein. Nomenclature deviated from that used in the report proper with respect to station numbers, which are defined in Figure B1, and angles, which are defined in Figure B2. Those parameters used solely in this appendix are defined as appropriate.

1. Blading Efficiency

Definition*:

$$\frac{V_1^2}{2g_o\mathcal{J}} = \eta_n \left(\Delta h'_n + \frac{V_o^2}{2g_o\mathcal{J}}\right) \; ; \quad \frac{W_2^2}{2g_o\mathcal{J}} = \eta_r \left(\Delta h'_r + \frac{W_1^2}{2g_o\mathcal{J}}\right) \qquad (1)$$

where:

$$\eta_n \text{ or } \eta_r = 1 - \zeta = 1 - (\zeta_p + \zeta_w + \zeta_r + \zeta_{zus}) \qquad (2)$$

with:

ζ = Total loss coefficient

ζ_p = Profile loss coefficient

ζ_w = Wall loss coefficient

ζ_r = Secondary loss coefficient

ζ_{zus} = Damping wire loss coefficient (not used for M-1 turbine)

The profile loss coefficient ζ_p is obtained from:

$$\zeta_p = \zeta_{po} \cdot \chi_p \cdot \chi_m \cdot \chi_\delta + \zeta_m + \zeta_F \qquad (3)$$

with*: $\zeta_{po} = f(\alpha_o \; ; \; \alpha_1)$ from Figure B3

*For the rotor, the absolute angles should be replaced by the relative angles and the flow conditions at the stator exit by the flow conditions at the rotor exit.

(1) Traupel, Walter, Thermische Turbomaschinen, Erster Band, Springer Verlag, Berlin/Goettingen, Heidelberg, 1958, Pages 269 through 298.

$$\chi_{po} = f\left(\frac{V_1 c\, \rho_1}{\mu_1} \;;\; ks/c\right) \qquad \text{from Figure B5}$$

$$\chi_m = f\,(V_1/a_1^*) \qquad \text{from Figure B4}$$

$$\chi_\delta = f\,(1 - f) \qquad \text{from Figure B6}$$

$$\zeta_m = f\,(1 - f) \qquad \text{from Figure B6}$$

$$\zeta_F = f\,(h/D_m) \qquad \text{from Figure B7}$$

The wall loss coefficient ζ_w, which is due to the friction loss on hub and tip annuli, is estimated as follows:*

$$\zeta_w = \zeta_{po}\, \chi_p\, \frac{s_1 \sin\alpha_1}{h} + C_f\, \frac{\Delta b}{h \cdot \sin\alpha_1}\, \gamma \qquad (4)$$

The second term gives the loss due to gas friction in the gap between stator and rotor. It usually is negligible.

For the secondary loss coefficient ζ_r we set:

$$\zeta_r = \chi_\ell \zeta_{ro} + \zeta_s \qquad (5)$$

with:* $\zeta_{ro} = f\,(\varphi_1 = \frac{V_1 \sin\alpha_1}{U_1})$ from Figure B8**

$\chi_\ell/\chi_p = f\,(c/h)$ from Figure B9

$\zeta_s = f\,(h_s/h)$ from Figure B10 (not applicable for present design)

*See footnote on Page B1.

**In Figure B8 the band for $\zeta_{ro} = f\,(\varphi)$ was extrapolated. The band was assumed to become horizontal, similar to the loss coefficients given in VAVRA.

The dampening wire loss coefficient ζ_{zus} is obtained from:*

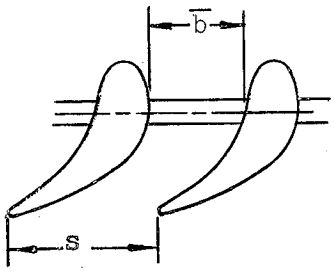

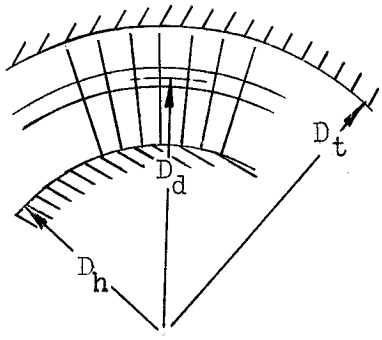

$$\zeta_{zus} = 4\, C_w \left(\sin\alpha\right)^2_1 \left(\frac{s}{b}\right)^2 \frac{D_d \cdot d}{D_t^2 - D_h^2} \qquad (6)$$

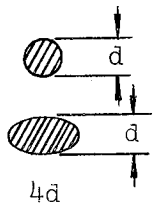

$C_w = 1.2 - 2.4$

$C_w = .4 - .8$

2. Velocity Triangle Efficiency

With η_n and η_r or K_n and K_r ($\eta = K^2$) known, the velocity triangle can be calculated and with it the velocity triangle efficiencies:

$$\eta_{su} = \Delta h/\Delta h' \qquad \text{Static to static} \qquad (7)$$

$$\eta_u = \frac{Lu}{\Delta h' + \frac{V_o^2 - V_2^2}{2g_o\mathcal{J}}} = \frac{\Delta h + \frac{V_o^2 - V_2^2}{2g_o\mathcal{J}}}{\Delta h' + \frac{V_o^2 - V_2^2}{2g_o\mathcal{J}}} \qquad \text{Total to total} \qquad (8)$$

$$\eta_u^* = \frac{Lu}{\Delta h' + V_o^2/2g_o\mathcal{J}} = \frac{\Delta h + \frac{V_o^2 - V_2^2}{2g_o\mathcal{J}}}{\Delta h' + V_o^2/2g_o\mathcal{J}} \qquad \text{Total to static} \qquad (9)$$

3. Stage Efficiency

The internal or stage efficiencies are defined as follows:

*See footnote on Page B1.

$$\eta_{si} = \frac{\Delta h - \Sigma \Delta L}{\Delta h'} = \frac{\Delta h}{\Delta h'} - \frac{\Sigma \Delta L}{\Delta h'} = \eta_{su} - \Sigma\zeta$$

$$\eta_{si} = \eta_{su} - (\zeta_{Ln} + \zeta_{Lr} + \Sigma\zeta_R + \zeta_v + \zeta_B) \quad \text{Static to static} \quad (10)$$

With:

ζ_{Ln} = Leakage loss coefficient for nozzle (stator)

ζ_{Lr} = Leakage loss coefficient for rotor

$\Sigma\zeta_R$ = Sum of disc - and shroud friction loss coefficients

ζ_v = Blade windage loss coefficient

ζ_B = Moisture loss coefficient (not applicable for present design)

As in section 2 the following additional efficiencies are defined

$$\eta_i = \eta_u - (\zeta_{Ln} + \zeta_{Lr} + \Sigma\zeta_R + \zeta_v + \zeta_B) \frac{\Delta h'}{\Delta h' + \frac{V_o^2 - V_2^2}{2g_o J}}$$

total to total (11)

$$\eta_i^* = \eta_u^* - (\zeta_{Ln} + \zeta_{Lr} + \Sigma\zeta_R + \zeta_v + \zeta_B) \frac{\Delta h'}{\Delta h' + V_o^2/2g_o J}$$

total to static (12)

The leakage loss coefficients ζ_{Ln}, ζ_{Lr} for blades without shrouds are calculated from:

$$\zeta_{Ln} = K_I \frac{A_{Ln}}{\Omega_1 \sin\alpha_1}, \quad \zeta_{Lr} = K_I \frac{A_{Lr}}{\Omega_2 \sin\beta_2} \quad (13)$$

With*: $K_I = f(\Delta\alpha)$ from Figure B11

*See footnote page B1.

A_L = Leakage area (A_{Ln}, nozzle; A_{Lr}, rotor)

Ω = Annulus area $= \pi Dh$

and for blades with shrouds from:

$$\zeta_{Ln} = \frac{K_{II}}{\sqrt{Z_n}} \quad \frac{A_{Ln}}{\varepsilon \Omega_1 \sin\alpha_1} \; ; \quad \zeta_{Lr} = \frac{K_{II}}{\sqrt{Z_r}} \quad \frac{A_{Lr}}{\Omega_2 \sin\beta_2}$$

With*:

Z = Number of laybrinths

ε = arc of admission

$K_{II} = f\,(\Delta h'/V_1^2/2g_o\mathcal{J})$ from Figure B12

The loss coefficients ζ_R for disc - and shroud friction are expressed by equations (15) and (16).

$$\zeta_R = \frac{2.54\ C_M}{\varepsilon} \quad \frac{(D_h/D_m)^4 \ (D_h/h)}{\varphi\psi} \qquad \text{(Disc)} \qquad (15)$$

$$\zeta_R = \frac{C_f\ (D_t/D_m)^4\ (b/h)}{\varphi\psi} \qquad \text{(Shroud)} \qquad (16)$$

With:

$C_M = f\,(Re_{C_m} = \frac{D_h\ U_h\ \rho}{\mu})$ from Figure B5

$$\varphi = \frac{V_x}{U} = \frac{\dot{m}}{U_2\ \varepsilon\Omega_2\ \rho_2}$$

$$\psi = \Delta h'/(U^2/2g_o\mathcal{J})$$

$C_f = f\,(Re_{C_f} = \frac{U_t\ \delta\ \rho}{\mu})$ from Figure B5

*See footnote page B1.

The blade windage loss coefficient ζ_v can be calculated from equation (17)

$$\zeta_v = C \frac{1 - \varepsilon}{\varepsilon \varphi \psi} + \frac{.30 \, Z_b}{\varepsilon \sqrt{\psi}} \frac{b}{D_m} \qquad (17)$$

With:

$C = .04 + .52 \, h/Dm$ blades free, upstream

$C = .019 + 1.1 \, (.125 - h/Dm)^2$ blades covered, upstream

$C = .88 - 13 \, (h/Dm)^2$ blades free, downstream

$C = .02 + 3.0 \, (.125 - h/Dm)^2$ blades covered downstream

Z_b : number of admission segments which result in the total admission ε. Make if possible $Z_b = 1$.

Frequently it is convenient to calculate the power loss due to friction (N_R) or ventilation (N_V), rather than the loss coefficient ζ_R or ζ_v.

$$N_R = 4 \, C_M \frac{\rho}{g_o} U_m^3 \, (D_h/D_m)^3 \, D_h^2 \qquad (18)$$

$$N_V = \frac{\pi}{2} \, C \, (1 - \varepsilon) \frac{\rho}{g_o} D_m \, h \, U_m^3 \qquad (19)$$

The moisture losses being negligible in the present application are not discussed further.

According to Ref. 3 the loss system described above is applicable to subsonic turbines having blades of the general shape of Figure B1 with a solidity according to Figure B2.

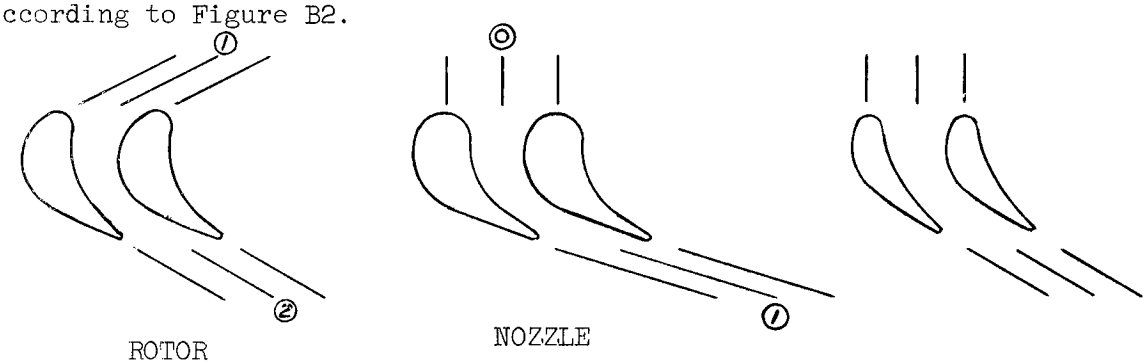

FIGURE B1

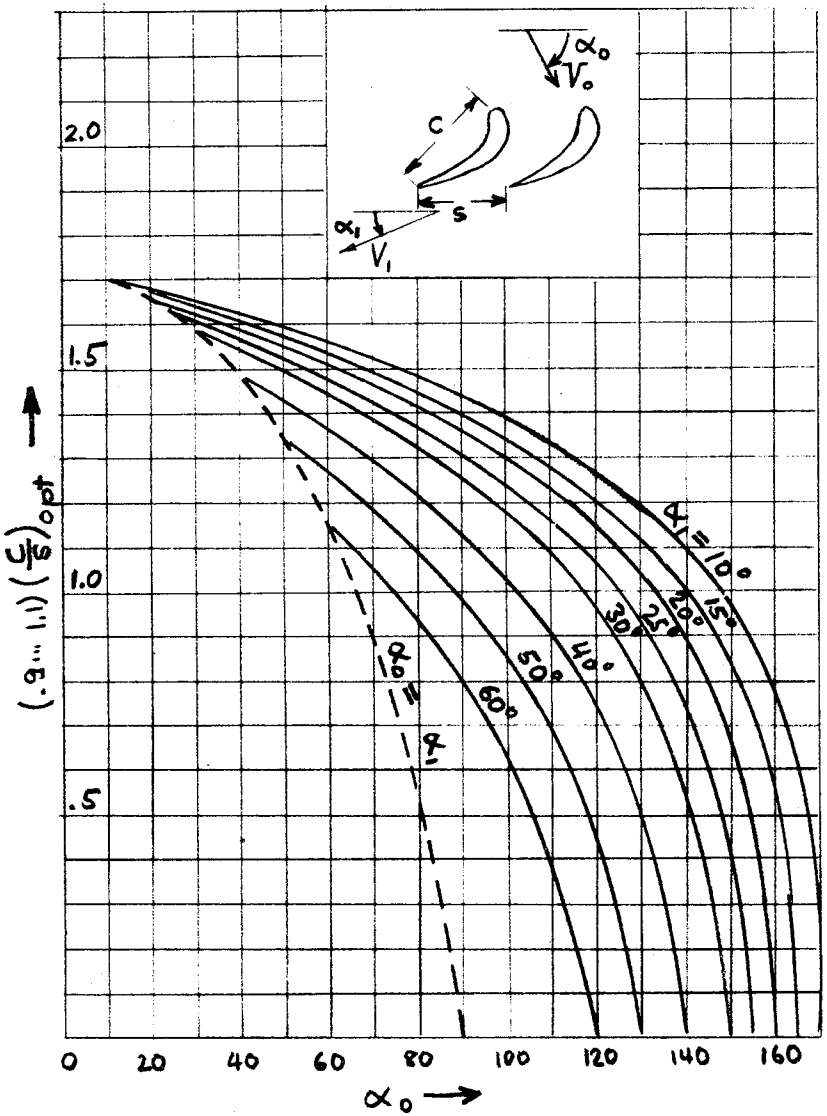

FIGURE B2 OPTIMUM SOLIDITY $\sigma = C/S$.

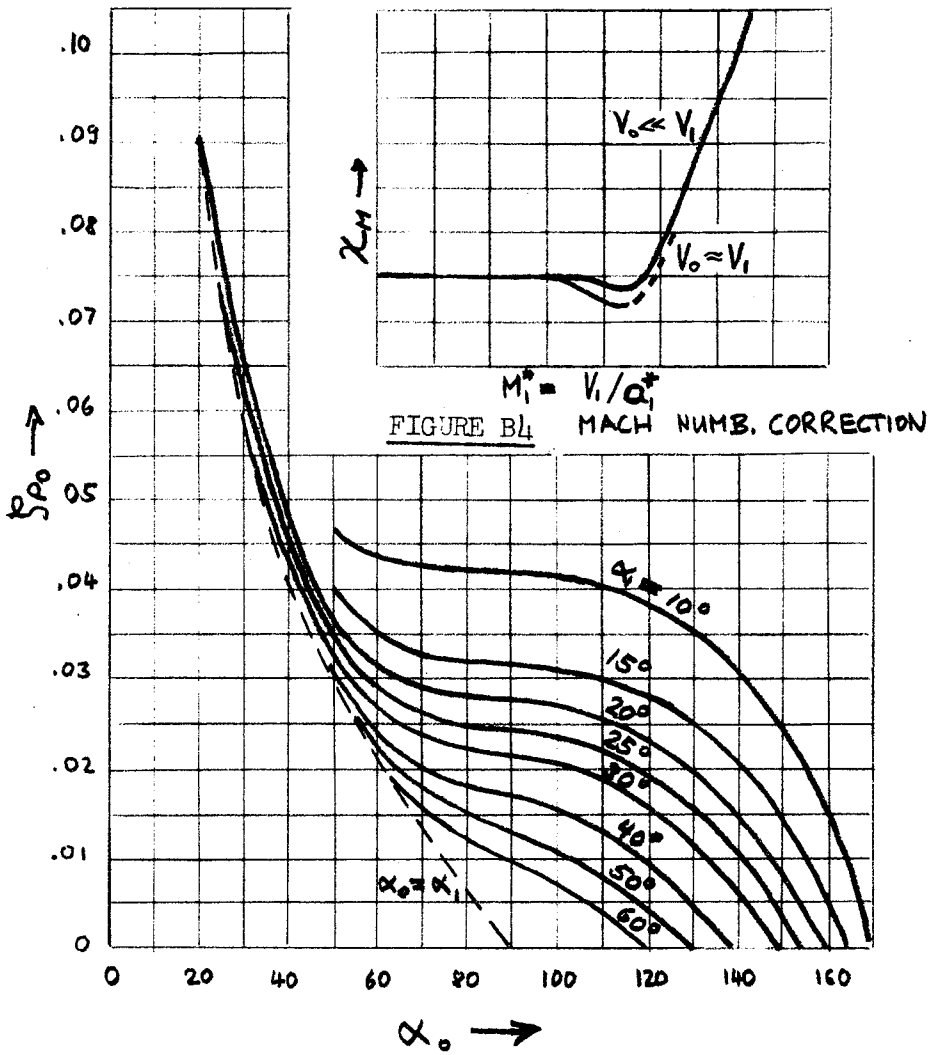

FIGURE B3 BASIC PROFIL LOSS ζ_{P_0}.

FIGURE B4 MACH NUMB. CORRECTION

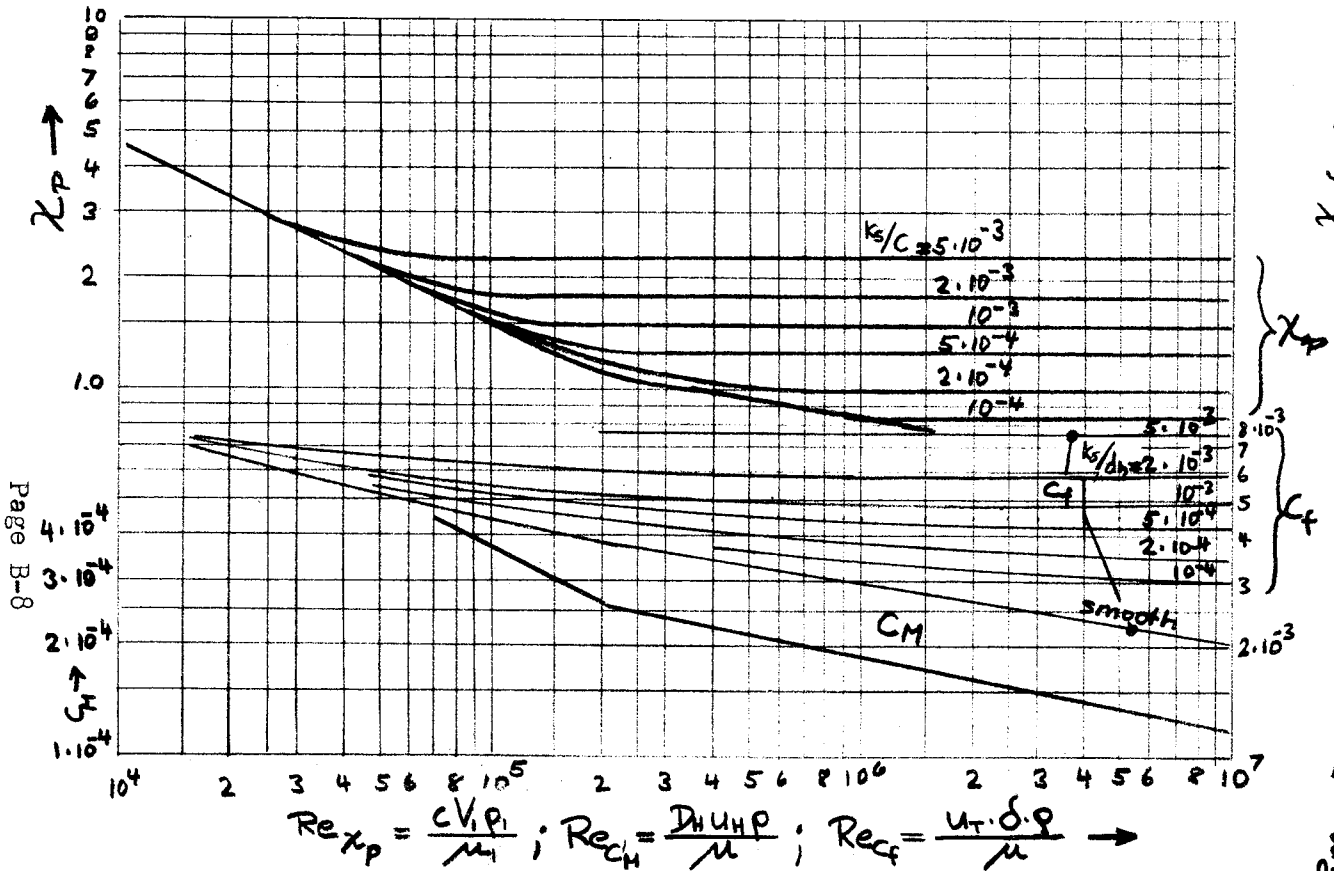

FIGURE B5 RENOLDS NUMBER CORRECTION χ_p.
DISC FRICTION COEFFICIENT C_M.
SHROUD FRICTION COEFFICIENT C_f.
(δ DISTANCE BETWEEN SHROUD AND HOUSING).

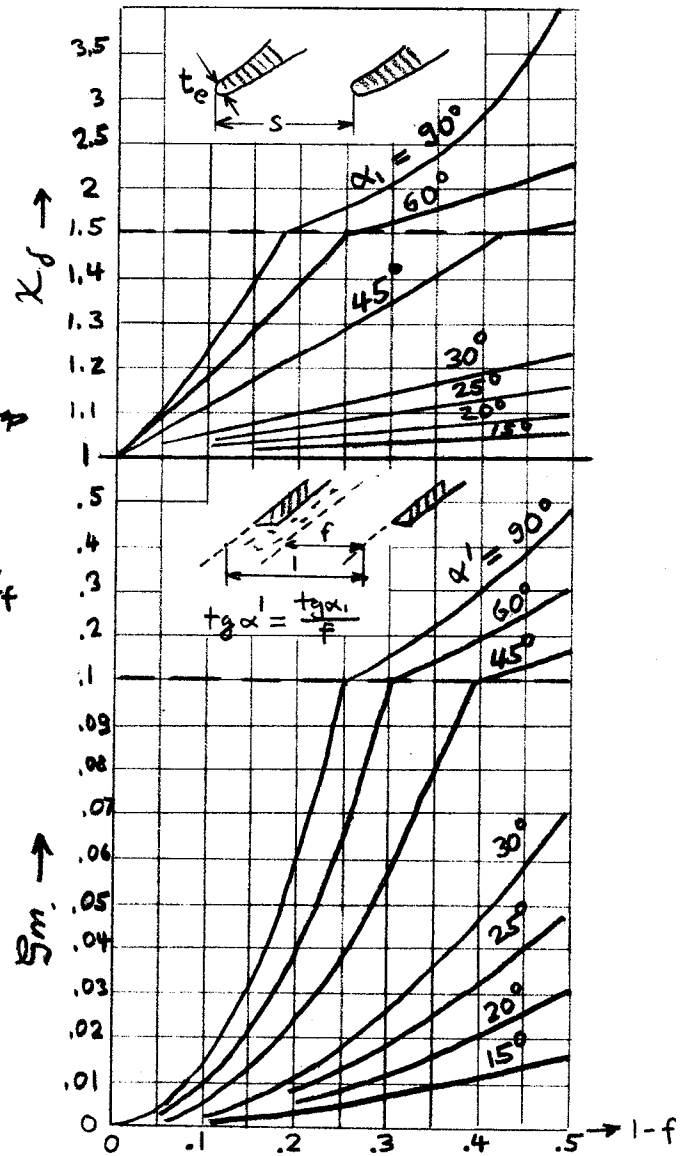

FIGURE B6 TRAILING EDGE, (χ_δ) AND SEPARATION, (ζ_m) LOSSES.
$1-f = t_e/(s\cdot\sin\alpha_1)$

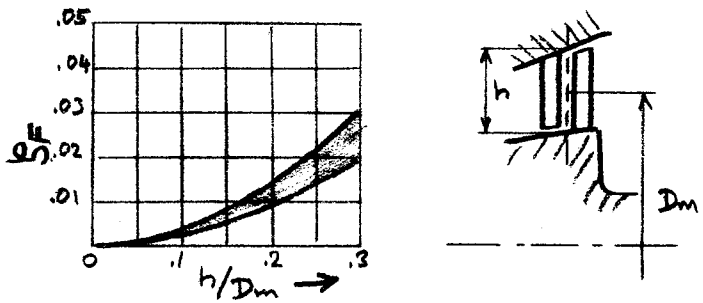

FIGURE B7 LOSS DUE TO STRAIGHT, NOT TWISTED BLADES ζ_F.

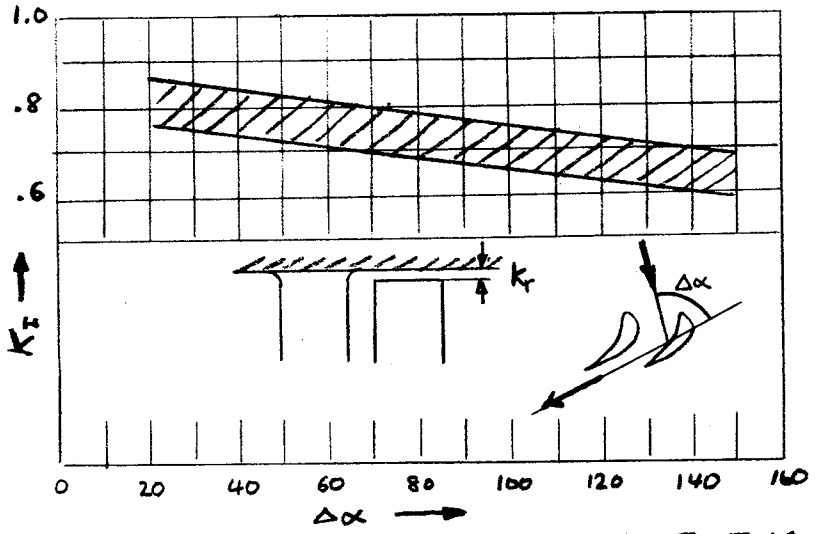

FIGURE B11 LEAKAGE LOSS COEFFICIENT K_I

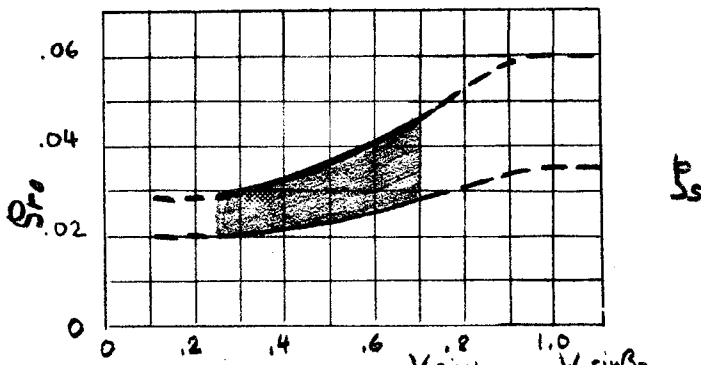

FIGURE B8 $\varphi_1 = \frac{V_1 \sin\alpha_1}{U_1}$; $\varphi_2 = \frac{W_2 \sin\beta_2}{U_2}$ →

BASIC SECONDARY LOSS ζ_{ro}.

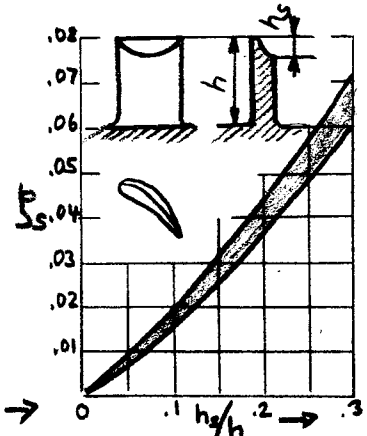

FIG. B10 TIP Loss ζ_s

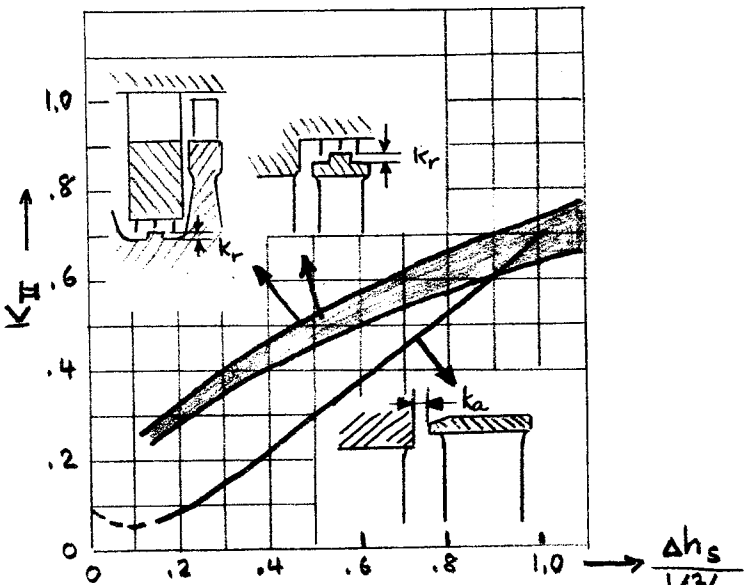

FIGURE B12 LEAKAGE LOSS COEFFICIENT K_{II}

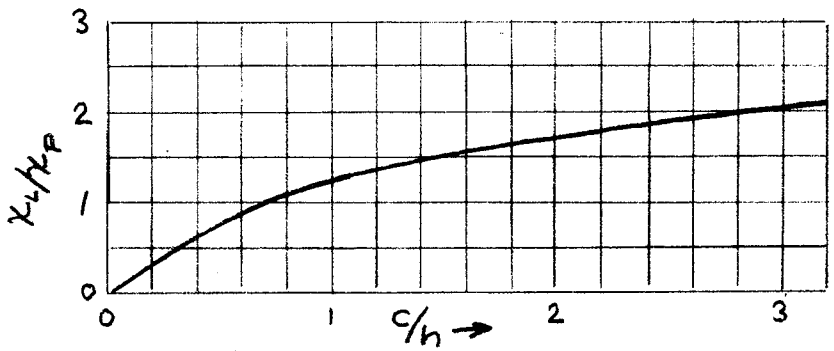

FIGURE B9 ASPECT RATIO CORRECTION χ_L/χ_p

REPORT NASA CR 54764 DISTRIBUTION LIST

W. F. Dankhoff (3 Copies)
NASA
Lewis Research Center
21000 Brookpark Road
Cleveland, Ohio 44135
Mail Stop 500-305

J. A. Durica (1 Copy)
Mail Stop 500-210

Patent Counsel (1 Copy)
Mail Stop 77-1

Lewis Library (2 Copies)
Mail Stop 3-7

Lewis Technical Information
Division (1 Copy)
Mail Stop 5-5

M. J. Hartmann (1 Copy)
Mail Stop 5-9

W. L. Stewart (1 Copy)
Mail Stop 5-9

J. C. Montgomery (1 Copy)
Mail Stop 501-1 SNPO-C

Major E. H. Karalis (1 Copy) AFSC Liaison Office
Mail Stop 4-1

Lewis Office of Reliability and
Quality Assurance (1 Copy)
Mail Stop 500-203

NASA Representative (6 Copies)
NASA Scientific and Technical
Information Facility
Box 5700
Bethesda, Maryland

Library (1 Copy)
NASA
Ames Research Center
Moffett Field, California 94035

Library (1 Copy)
NASA
Flight Research Center
P. O. Box 273
Edwards AFB, California 93523

Library (1 Copy)
NASA
Goddard Space Flight Center
Greenbelt, Maryland 20771

Library (1 Copy)
NASA
Langley Research Center
Langley Station
Hampton, Virginia 23365

Library (1 Copy)
NASA
Manned Spacecraft Center
Houston, Texas 77058

Library (1 Copy)
NASA
George C. Marshall Space Flight Center
Huntsville, Alabama 35812

Library (1 Copy)
NASA
Western Operations
150 Pico Boulevard
Santa Monica, California 90406

Library (1 Copy)
Jet Propulsion Laboratory
4800 Oak Grove Drive
Pasadena, California 91103

A. O. Tischler (2 Copies)
NASA Headquarters
Code RP
Washington, D. C.

L. E. Baughman (1 Copy)
Aerojet-General Corporation
Liquid Rocket Operations
NASA Plant Representative
Building 2001, Room 53
Sacramento, California 95809

J. W. Thomas, Jr. (5 Copies)
NASA
George C. Marshall Space Flight
Center I-E-E
Huntsville, Alabama

E. W. Gomersall (1 Copy)
NASA
Mission Analysis Division
Office of Advanced Research and
Technology
Moffett Field, California 94035

Dr. Keith Boyer (1 Copy)
Los Alamos Scientific Laboratory
CMF-9
P. O. Box 1663
Los Alamos, New Mexico

A. Schmidt (1 Copy)
National Bureau of Standards
Cryogenic Division
Boulder, Colorado

Dr. G. Wislicenus (1 Copy)
Penn State University
Naval Ordinance Laboratory
University Park, Pennsylvania

Dr. A. Acosta (1 Copy)
California Institute of Technology
1201 East California Street
Pasadena, California

Dr. E. B. Konecci (1 Copy)
National Aeronautics and Space Council
Executive Office of the President
Executive Office Building
Washington, D. C.

Dr. M. Vavra (1 Copy)
Naval Post Graduate School
Monterey, California

H. V. Main (1 Copy)
Air Force Rocket Propulsion Laboratory
Edwards Air Force Base
Edwards, California

Dr. George Serovy (1 Copy)
Iowa State University
Ames, Iowa

T. Iura (1 Copy)
Aerospace Corporation
2400 East El Segundo Blvd.
P. O. Box 95085
Los Angeles, California 90045

REPORT NASA CR 54764 DISTRIBUTION LIST

(Continued)

F. Ghahnemani (1 Copy)
Aerospace Corporation
2400 East El Segundo Blvd.
P. O. Box 95085
Los Angeles, California 90045

Chemical Propulsion Information Agency (1 Copy)
Johns Hopkins University
Applied Physics Laboratory
8621 Georgia Avenue
Silver Spring, Maryland

Robert O. Bullock (1 Copy)
Garrett Corporation
Airesearch Manufacturing Division
402 S. 36th Street
Phoenix, Arizona 85034

Pratt and Whitney Aircraft Corporation
(1 Copy)
Florida Research and Development Center
P. O. Box 2691
West Palm Beach, Florida 33402

Rocketdyne (Library Department
586-306) (1 Copy)
Division of North American Aviation
6633 Canoga Avenue
Canoga Park, California 91304

John Stanitz (1 Copy)
Thompson-Ramo-Wooldridge, Inc.
23555 Euclid Avenue
Cleveland, Ohio 44117

Dr. M. J. Zucrow (1 Copy)
Purdue University
Lafayette, Indiana 47907